Measurement of the form factors in the decay $K_L^0 \to \pi\mu\nu$†

G. Donaldson, D. Fryberger, D. Hitlin, J. Liu, B. Meyer,* R. Piccioni,‡ A. Rothenberg,§ D. Uggla, and S. Wojcicki‖

Physics Department and Stanford Linear Accelerator Center, Stanford University, Stanford, California 94305

D. Dorfan‖

Physics Department, University of California, Santa Cruz, California 95064

(Received 12 November 1973)

A Dalitz plot of 1.6×10^6 $K_L^0 \to \pi\mu\nu$ decays has been studied to measure the t dependence of the vector and scalar form factors. The observed slopes, $\lambda_+ = 0.030 \pm 0.003$ and $\lambda_0 = 0.019 \pm 0.004$, are compatible with current-algebra and soft-pion predictions, μ-e universality, and $K^*(890)$ dominance of the vector form factor.

I. INTRODUCTION

The study of the t dependence of the form factors in the semileptonic decays of the K meson provides unique information about the symmetry properties and the dynamics of the strong interactions. Thus, the field of K_{l3} decays has become a popular testing ground for ideas such as current algebra, PCAC (partially conserved axial-vector current), chiral symmetry, and different analyticity and unitarity assumptions about the axial-vector currents. In this paper we shall describe in detail a high-statistics measurement (1.6 million events) of the Dalitz plot in $K_L^0 \to \pi\mu\nu$ decay, and compare the results with the predictions which follow from several different theoretical *Ansätze*, as well as with previous form factor determinations based on K_{e3} decay rate and Dalitz-plot measurements, and $K_{\mu 3}$ decay rate, Dalitz plot, and muon polarization measurements, for both K^+ and K_L^0 decays.

This experiment was performed concurrently with the measurement of the charge asymmetry in $K_L^0 \to \pi^\pm\mu^\mp\nu$ decay, which has been described in the previous paper, hereinafter referred to as paper I.[1] A brief description of the present experiment has also been published previously.[2] Minor improvements in the analysis have resulted in small changes in the results as presented in Ref. 2. Our conclusions remain unchanged, however, and the present results represent the final analysis of this experiment. The reader is referred to paper I, and to a previous report on the data acquisition system of the Stanford Linear Accelerator Center (SLAC) K^0 spectrometer[3] for a complete description of the experimental apparatus.

II. EXTRACTION AND PARAMETRIZATION OF THE FORM FACTORS

We shall assume the validity of the current-current picture of the semileptonic strangeness-changing weak interactions. The most general matrix element for K_{l3} decay may then be written as

$$\mathfrak{M} = \frac{G}{\sqrt{2}} \sin\theta_C \Big[f_+(t)(p_K + p_\pi)^\mu \bar{u}_l \gamma_\mu (1+\gamma_5) u_\nu + f_-(t)(p_K - p_\pi)^\mu \bar{u}_l \gamma_\mu (1+\gamma_5) u_\nu + m_K f_S \bar{u}_l (1+\gamma_5) u_\nu + \frac{f_T}{2m_K} (p_K^\lambda p_\pi^\mu - p_K^\mu p_\pi^\lambda) \bar{u}_l \sigma_{\lambda\mu} (1+\gamma_5) u_\nu \Big], \tag{1}$$

where θ_C is the Cabibbo angle, f_+ and f_- are the vector form factors, and f_S and f_T are the scalar and tensor form factors, respectively. Time-reversal invariance ensures that the form factors are relatively real, while local creation of the lepton pair requires that they be functions only of the square of the four-momentum transfer to the leptons

$$t = (p_K - p_\pi)^2 = m_K^2 + m_\pi^2 - 2p_K \cdot p_\pi .$$

The physical decay region is bounded by $m_l^2 < t < (m_K - m_\pi)^2$.

The density of events on the Dalitz plot is given by[4]

$$\frac{d^2N(E_\pi^*, E_l^*)}{dE_\pi^* dE_l^*} = \frac{G^2 \sin^2\theta_C}{16\pi^3} \times \left[|F_1|^2 E_\pi' + |F_2|^2 m_K (2E_l^* E_\nu^* - m_K E_\pi') + 2\,\mathrm{Re}\, F_1 F_2^* m_l E_\nu^* \right], \tag{2}$$

where

$$F_1 = m_l(f_- - f_+) + m_K f_S - (E_l^* - E_\nu^*) f_T,$$
$$F_2 = 2f_+ + \frac{m_l}{m_K} f_T. \tag{3}$$

E_π^*, E_l^*, and E_ν^* are respectively the pion, lepton, and neutrino energies in the kaon center-of-mass system,[5] and

$$E'_\pi = E_\pi^{*\max} - E_\pi^* = \frac{m_K^2 + m_\pi^2 - m_l^2}{2m_K} - E_\pi^*. \tag{4}$$

Figure 1 shows the $K_{\mu 3}$ Dalitz-plot distributions for pure vector, scalar, and tensor couplings. Similar distributions for K_{e3} decay may be found in the review article by Chounet, Gaillard, and Gaillard,[4] which we shall henceforth refer to as CGG.

All the information on the strangeness-changing weak current obtainable from the study of K_{l3} decays is contained in the t dependence of the form factors. According to the assumptions of the Cabibbo theory, only vector coupling contributes to the matrix element and the Dalitz-plot density reduces to the simpler expression

$$\frac{d^2N(E_\pi^*, E_l^*)}{dE_\pi^* dE_l^*} = \frac{G^2 \sin^2\theta_C}{4\pi^3} \times [Af_+(t)^2 + Bf_+(t)f_-(t) + Cf_-(t)^2], \tag{5}$$

where

$$A = m_K(2E_l^* E_\nu^* - m_K E'_\pi) + m_l^2(\tfrac{1}{4}E'_\pi - E_\nu^*),$$
$$B = m_l^2(E_\nu^* - \tfrac{1}{2}E'_\pi), \tag{6}$$
$$C = \tfrac{1}{4}m_l^2 E'_\pi.$$

A least-squares fit of the experimentally determined Dalitz-plot density to this distribution provides a test of the assumption of pure vector coupling and serves to determine the t dependence of the form factors. It has been customary to analyze K_{l3} decay experiments in terms of the form factors $f_+(t)$ and $\xi(t) \equiv f_-(t)/f_+(t)$. We have given primary consideration, however, to a different combination of form factors, namely, $f_+(t)$ and

$$f_0(t) = f_+(t) + \frac{t}{m_K^2 - m_\pi^2} f_-(t), \tag{7}$$

which are the amplitudes corresponding to 1^- (vector) and 0^+ (scalar) exchange, respectively. These form factors are more directly related to theoretical predictions, and are less strongly correlated than f_+ and ξ.

Historically, f_+ and f_- were assumed to have linear t dependence. We have, however, analyzed the Dalitz plot in terms of f_+ and f_0, the amplitudes which have definite spin and parity, and have assumed that it is these amplitudes which have linear t dependence:

$$f_+(t) = f_+(0)\left(1 + \lambda_+ \frac{t}{m_\pi^2}\right),$$
$$f_0(t) = f_0(0)\left(1 + \lambda_0 \frac{t}{m_\pi^2}\right). \tag{8}$$

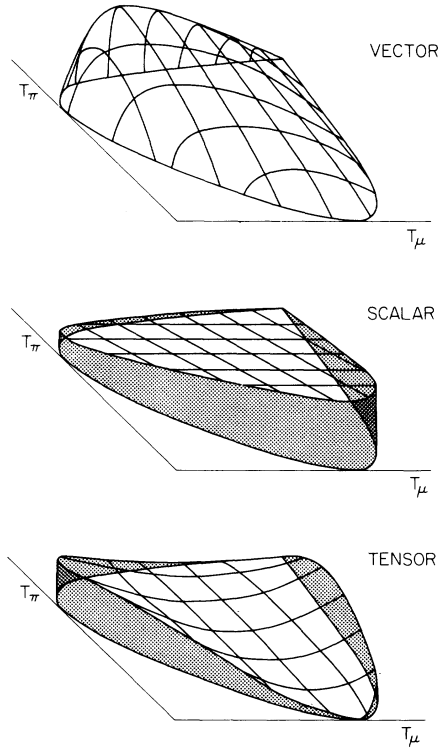

FIG. 1. Dalitz-plot density distributions for $K_{\mu 3}$ decay for pure vector, scalar, and tensor couplings. The shaded areas denote the value of $|\mathfrak{M}|^2$ at the kinematic boundary.

Note that this expansion is inconsistent with a linear expansion of f_-:

$$f_-(t) = f_-(0)\left(1 + \lambda_- \frac{t}{m_\pi^2}\right). \tag{9}$$

That is, from this point of view, we have $\lambda_- = 0$. The t dependence of the ξ form factor is then likely to be slight,

$$\xi(t) = \frac{m_K^2 - m_\pi^2}{m_\pi^2} \frac{(\lambda_0 - \lambda_+)}{(1 + \lambda_+ t/m_\pi^2)}, \tag{10}$$

and the parameter $\xi(0)$ is given by

$$\xi(0) = \frac{m_K^2 - m_\pi^2}{m_\pi^2}(\lambda_0 - \lambda_+). \tag{11}$$

Since the form factors are functions only of $t = m_K^2 + m_\pi^2 - 2m_K E_\pi^*$, and therefore of E_π^*, it is

also possible to determine their t dependence without prior parametrization by fitting the vector shape (quadratic in E_μ^*) to events in a band of constant E_π^* on the Dalitz plot. In this way, a plot is made of f_+ and f_0 (or ξ) as a function of t, and the t dependence of these form factors is directly ascertained by a least-squares fit of an assumed functional form: polynomial, dipole, etc. This procedure has the disadvantage that since each form factor is fitted independently to a given functional form, the resulting parameters tend to be more poorly determined, and are more susceptible to systematic errors than parameters determined by a parametrized fit to the entire Dalitz plot. This problem is discussed in more detail in Sec. VII.

III. THEORETICAL PREDICTIONS FOR THE FORM FACTORS

The great interest in the study of the form factors in K_{l3} decay arises because of the possibility of testing a rather straightforward series of predictions which follow from dispersion relations, the existence of current algebra, and the hypothesis of PCAC in its several forms.

The vector form factor is expected to obey a dispersion relation with at most one subtraction. If the $f_+(t)$ amplitude is unsubtracted, then approximation of the dispersion integral with 1^- poles leads to what is called K^* dominance, i.e.,

$$f_+(t) = f_+(0)\frac{m_{K^*}{}^2}{m_{K^*}{}^2 - t}\ , \tag{12}$$

since the $K^*(890)$ is the only known 1^- strange meson. If one then uses a linear parametrization of $f_+(t)$ in the physical region, an experiment with uniform detection efficiency as a function of t would find $\lambda_+ = 0.029$. An experiment whose sensitivity is greatest at low t would produce a result closer to the threshold value $\lambda_+ = 1/m_{K^*}{}^2 = 0.245$, while an experiment with greatest sensitivity at high t would find $\lambda_+ > 0.029$. If, on the other hand, $f_+(t)$ is once subtracted, then even if the integral is saturated by the $K^*(890)$, there is one additional subtraction constant, and the t dependence of f_+ is undefined.

If the scalar form factor also obeys an unsubtracted dispersion relation, then its t dependence will be approximated by 0^+ poles. There is no definite candidate for a 0^+ pole, although there is some evidence that the $K\pi$ S-wave phase shift goes through 90° in the 1200–1400 MeV region.[6] On this basis, one might then expect f_0 to have a smaller slope than f_+, i.e., $\lambda_0 < \lambda_+$.

Information on the t dependence of f_0 can, however, be obtained using current algebra and PCAC. An attractive scheme in which current algebra and pion PCAC notions are connected is one in which chiral $SU(2)\otimes SU(2)$ symmetry of the charges associated with the weak hadronic currents is realized through a Goldstone-boson mechanism. An immediate consequence of this symmetry is the Callan-Treiman relation,[7] which we quote here in a form which is explicitly good to first order in $SU(2)\otimes SU(2)$ symmetry breaking[8,9]:

$$\begin{aligned} f_0(m_K{}^2 - m_\pi{}^2) &= f_+(m_K{}^2 - m_\pi{}^2) + f_-(m_K{}^2 - m_\pi{}^2) \\ &= f_K/f_\pi \\ &= (1.25 \pm 0.03) f_+(0)\ . \end{aligned} \tag{13}$$

An extension of these chiral symmetry ideas has been made by Dashen and Weinstein,[8] who assume that $SU(3)\otimes SU(3)$ is a symmetry of the hadrons, and that this symmetry is realized through a mechanism in which all the pseudoscalar mesons are Goldstone bosons. A direct prediction of this idea, valid to first order in $SU(3)\otimes SU(3)$ breaking and independent of the mechanism of symmetry breaking, is that the slope of the scalar form factor at the unphysical point $t = m_K{}^2 + m_\pi{}^2$ is given by

$$\begin{aligned} \lambda_0 &= m_\pi{}^2 \frac{df_0}{dt}\Big|_{t = m_K{}^2 + m_\pi{}^2} \\ &= \frac{m_\pi{}^2}{2(m_K{}^2 - m_\pi{}^2)}\left(\frac{f_K}{f_\pi} - \frac{f_\pi}{f_K}\right) \\ &= 0.020 \pm 0.003\ . \end{aligned} \tag{14}$$

Subsequent analysis has indicated that there may be small first-order corrections to this result,[10] but this is unlikely to be of serious concern in the analysis of experiments at their current level of precision. Renner and Wambach[10] have recently shown that this prediction for λ_0 should not be suppressed by more than 20% at low t if $SU(2)\otimes SU(2)$ remains a valid symmetry. Note also that a linear extrapolation of f_0 from $t = 0$ to the Callan-Treiman point requires $\lambda_0 = 0.021$.

The Callan-Treiman relation gives a value for f_0 at an unphysical point, leading to the equivalent result for the ξ parameter at $t = m_K{}^2 - m_\pi{}^2$:

$$\xi(m_K{}^2 - m_\pi{}^2) = \frac{f_K/f_\pi}{f_+(m_K{}^2 - m_\pi{}^2)} - 1. \tag{15}$$

If we assume K^* dominance of an unsubtracted vector form factor, then $\xi(m_K{}^2 - m_\pi{}^2) = -0.09 \pm 0.03$. To make a statement about $\xi(0)$, we must make an assumption about the t dependence of f_0. Assuming a linear dependence, we obtain $\xi(0) = -0.11 \pm 0.03$. Thus the assumption of $SU(2)\otimes SU(2)$ symmetry implies that the ξ form factor is nearly independent of t.

Conflicting experimental evidence with regard to

these theoretical predictions has led to several attempts to find symmetry-breaking schemes which predict other values of the scalar form factor f_0 and its slope λ_0. This requires abandonment of either the PCAC hypothesis or current algebra itself. One such scheme assumes that when $SU(3) \otimes SU(3)$ is broken, $SU(3)$ remains as an approximate symmetry and that there is only a weak form of PCAC,[11] i.e., that the matrix element of the divergence of the axial-vector current between physical states is dominated by the pion at $t=0$. Brandt and Preparata,[11] using these assumptions, together with the technique of light-cone expansions to determine extrapolations off the mass shell, predict substantial modifications of the Callan-Treiman relation, to wit,

$$f_+(m_K^2) + f_-(m_K^2) \simeq 0.7 \frac{f_K}{f_\pi} , \tag{16}$$

or $\xi(0) \simeq -0.7$, assuming K^* dominance of $f_+(t)$. It appears, however, to be difficult to realize these results in a simple model.[12]

Since the current algebra and PCAC predictions refer to unphysical points, $t \simeq m_K^2$, the validity of extrapolations of the scalar form factor to $t \simeq m_K^2$ depends on its expected behavior in the physical region. A large number of papers have been written on this subject in an attempt to reconcile the Callan-Treiman prediction $f_0(m_K^2 - m_\pi^2)/f_+(0) = 1.25$ with evidence indicating that f_0 decreased with increasing t. Many of these approaches are very cogently summarized in the review of CGG,[4] but none of these attempts appears successful. Briefly, CGG concluded that the experimental situation, favoring a negative slope for $f_0(t)$ in the physical region, is incompatible with the smoothly rising t dependence predicted by soft-pion techniques, and that therefore $SU(2) \otimes SU(2)$ may not be a good symmetry of the strong interactions.

Recently a series of "rigorous bounds" on the t dependence of the form factors in the physical region have been derived.[13] The approaches are quite varied, but each author attempts to make minimal assumptions regarding the breaking of $SU(3) \otimes SU(3)$ or $SU(2) \otimes SU(2)$ symmetry, and then imposes the consequences of analyticity and various other assumptions on the spectral functions. Without exception, the conclusion is drawn that the validity of the soft-pion theorem requires $\lambda_0 > 0$ in the physical region.

Failure of the scalar form factor f_0 to extrapolate in value and slope to the Callan-Treiman and Dashen-Weinstein values, respectively, at $t \simeq m_K^2$ implies, if current algebra is a valid concept, that $SU(2) \otimes SU(2)$ is not a good symmetry of the strong interactions, and that strong PCAC is not valid for the pseudoscalar mesons. Such a failure may also, of course, imply that while the hadronic currents may exhibit $SU(3) \otimes SU(3)$ and $SU(2) \otimes SU(2)$ symmetry, it is not these currents which couple to leptons.

IV. APPARATUS

The experiment was performed at SLAC using the K^0 spectrometer, as shown in Fig. 2. We shall only give a brief description of the apparatus here since a full description has been presented in paper I.

A K_L^0 beam was produced by 19-GeV electrons incident on a 1-r.l. Be target. Under normal running conditions, there were 160 beams pulses per second, each 1600 nsec long and subdivided into 128 equally spaced buckets of <20 psec duration. A signal induced in a coaxial cable (the CABLE pulse) placed immediately downstream of the target provided the K_L^0 production time.

Two sets of 10-gap wire spark chambers, each containing $4X$, $4Y$, and two rotated UV readout planes, were placed on opposite sides of the spectrometer magnet, which had a field integral of 12.6 kG m. A veto counter V was followed by four hodoscope banks: T, A, B, and C. Behind the rear chambers was the muon filter, consisting of 7.7 interaction lengths of lead and 1 interaction length of paraffin. The paraffin was used to reduce the counting rates in the A, B, and C counters caused by the spray of low-energy neutrons from beam interactions in the lead wall. The decay volume, defined to be the space between the V and T counter banks, was 69 cm wide by 33 cm high. It was filled with helium, as was the space in the spectrometer magnet between the front and rear chambers. The incident K_L^0 flux at the center of the spectrometer magnet, 78.6 m from the production target, was $\sim 10^4$ K_L^0's per second. The trigger $\overline{V} \cdot 2T \cdot A \cdot B \cdot C \cdot$ CABLE required a charged decay product (presumably a muon) to penetrate

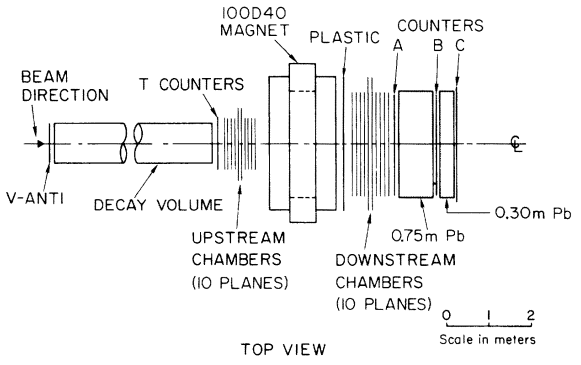

FIG. 2. SLAC K^0 spectrometer—plan view of the experimental apparatus.

both sections of the lead wall in order to trigger the B and C counters. The A, B, and C counters also served as timing counters. Together with the CABLE time, they provided us with a measurement of the K_L^0 time of flight (TOF) to an accuracy of $\pm\frac{1}{3}$ nsec over a flight path of about 75 m. The error in the determination of K_L^0 momentum is related to the TOF uncertainty by

$$\frac{\Delta P_K}{P_K} = \gamma^2 \frac{\Delta(\mathrm{TOF})}{\mathrm{TOF}} , \tag{17}$$

where $\gamma = E_K/m_K$. This corresponds to a $\Delta P_K/P_K$ of ±2% at $P_K = 2$ GeV/c, and ±25% at $P_K = 7$ GeV/c.

V. MONTE CARLO PROGRAM

The objective of the Monte Carlo program was to compute the detection efficiency of the experimental apparatus as a function of position on the $K_{\mu 3}^0$ Dalitz plot, as well as to provide a basis for comparison with the data in order to locate possible systematic errors. In principle, one could have recorded only the relevant details associated with each Monte Carlo event which satisfied the trigger, and started the analysis of Monte Carlo events at the level of PASS-3.[14] However, such a short-cut method would necessarily involve corrections for any biases introduced by using the PASS-1 and PASS-2 analysis programs on the experimental data. Since it was difficult to account for all of these biases, it was decided that the optimum procedure was to use the same set of analysis programs on the Monte Carlo data as was used on the experimental data. Accordingly, the output of the Monte Carlo program was made to consist of raw spark, latch, and analog-to-digital converter (ADC) data, written on magnetic tapes in the same format as experimental data. The subsequent Monte Carlo analysis paralleled the data analysis along each step of the way, from the grouping of sparks to form lines in PASS-1 to the application of the final cuts in PASS-3.

A. K_L^0 beam

A major problem encountered in any experiment involving a neutral beam is the determination of the beam spectrum. We extracted the K_L^0 decay momentum spectrum from the distribution of the sum of the energies of the charged pions in $K_{\pi 3}^0$ decays, with the help of the Monte Carlo.

We have isolated 39K predominantly $K_{\pi 3}^0$ events from a sample of data taken with a $\overline{V} \cdot 2T \cdot 2A \cdot$ CABLE trigger by applying the following cuts:

(a) $P_0'^2 < -0.004$ (GeV/c)^2,
(b) $P_\perp(\pi^+ \text{ and } \pi^-) < 0.135$ GeV/c,
(c) $P_\perp(\pi^0) < 0.130$ GeV/c,
(d) $m_{+-} < 0.365$ GeV/c^2,
where m_{+-} = mass of (π^+, π^-) system,
(e) no B or C counters latched.

The variable $P_0'^2$ (Ref. 15) is given by

$$P_0'^2 = \left[\frac{(m_K^2 - m_{+-}^2 - m_{\pi^0}^2)^2 - 4(m_{+-}^2 m_{\pi^0}^2 + m_K^2 P_\perp^2)}{4(P_\perp^2 + m_{+-}^2)}\right] , \tag{18}$$

where $P_\perp$ represents the transverse momentum of the (π^+, π^-) system relative to the direction of the K_L^0. The background of K_{l3}^0 events remaining after the above cuts was less than 5%.

An appropriate mixture of $K_{\pi 3}^0$, $K_{\mu 3}^0$, and K_{e3}^0 events was generated by the Monte Carlo program using the $\overline{V} \cdot 2T \cdot 2A$ trigger, resulting in a sample of 58K events after the same set of cuts (a)–(e). From these events, we determined $N(E_{+-}, P_K)$, a matrix describing the shape of the E_{+-} spectrum as a function of P_K, the laboratory momentum of the kaon. The shape of the K_L^0 decay momentum spectrum, $F(P_K)$, was then determined from the matrix equation $F = N^{-1}W$, where $W(E_{+-})$ is the experimentally observed E_{+-} spectrum. Figure 3 shows the shape of $N(E_{+-}, P_K)$ for various bands of P_K, and Fig. 4 shows the comparison between the experimental shape $W(E_{+-})$ and the Monte Carlo prediction. The latter was derived using the best-fit decay momentum spectrum as obtained from the matrix inversion technique described above. It should be pointed out that this method for deter-

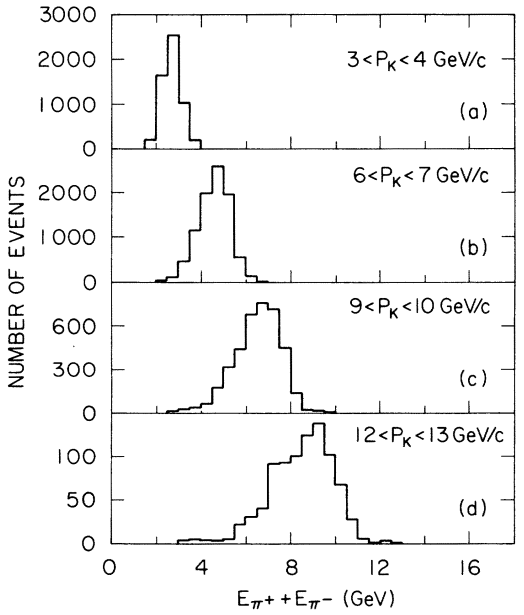

FIG. 3. The Monte Carlo predicted shape of the E_{+-} spectrum for events which satisfy the $K_{\pi 3}^0$ criteria as a function of P_K.

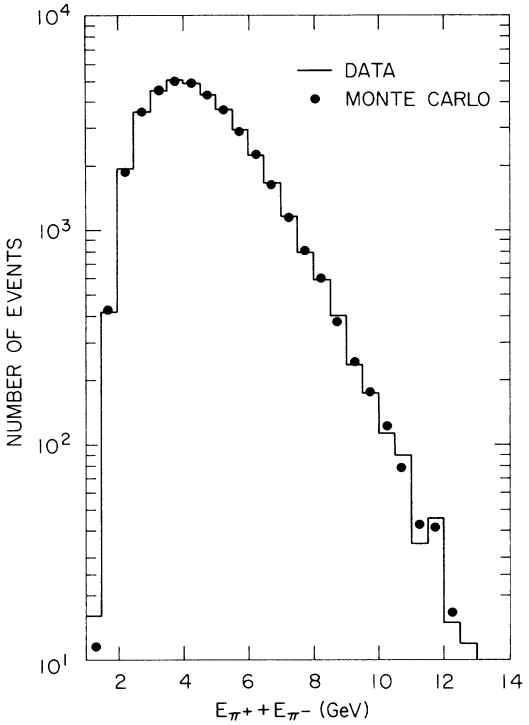

FIG. 4. The experimentally observed E_{+-} spectrum for all events, as compared with the Monte Carlo prediction obtained with a best-fit decay momentum spectrum.

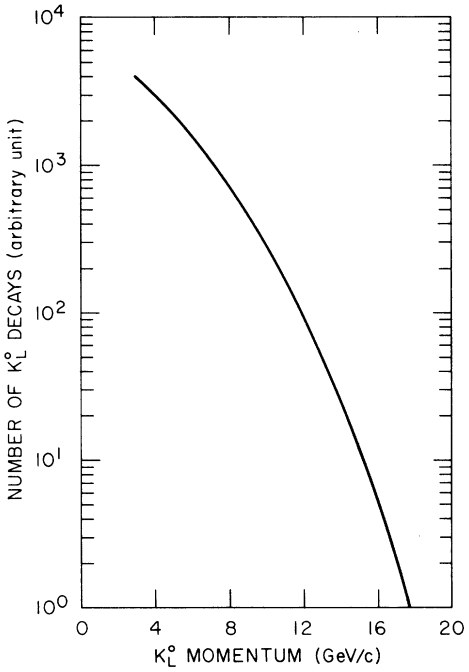

FIG. 5. The K_L^0 decay momentum spectrum.

mining the kaon decay momentum spectrum was independent of TOF measurements.

The statistics of the sample of $K_{\pi 3}^0$ events was such that a 2–3% accuracy was obtained near the peak of the decay momentum spectrum. However, at the low end of the spectrum (<3 GeV/c), where the spectrometer efficiency was very low, and at the high end of the spectrum (>12 GeV/c), where the number of K_L^0 decays was very small, the statistical accuracy was only ~10%. Therefore, we added small corrections to the spectrum in order to have good agreement between the experimental and Monte Carlo distributions of the reconstructed K_L^0 momentum for $K_{\mu 3}^0$ events (see Sec. VI C). The final corrected spectrum is shown in Fig. 5. The sensitivity of our final results to the shape of the K_L^0 decay momentum spectrum used in the Monte Carlo calculation is discussed in Sec. VIII A.

B. Beam scattering

There were approximately 1.5 interaction lengths of lead and 3 interaction lengths of polyethylene immediately after the production target to remove photons and reduce the neutron to K_L^0 ratio in the beam, respectively. An appreciable number of kaons were therefore diffractively scattered before reaching the decay volume. We have assumed the kaon diffractive cross section to be independent of energy and equal to $\frac{1}{3}$ of the total cross section, using collision lengths of 13.8 cm and 55 cm for lead and polyethylene, respectively. The scattering was assumed to have a t dependence of the form e^{-at}, with $a = 10$, 50, and 700 (GeV/c)$^{-2}$ for hydrogen, carbon, and lead, respectively.

The Monte Carlo calculation then indicates that roughly equal numbers of scattered and unscattered K_L^0's reached the decay volume. Although this estimate is expected to be accurate only to a factor of 2, it was adequate since the Monte Carlo calculation indicated that the observable differences between the diffractively scattered and unscattered events were negligible. Half the Monte Carlo events were thus generated with the K_L^0's coming from a point target, while the other half had kaons which came from a diffuse source at the position of the beam-defining collimator.

C. Decay modes generated

A total of four decay modes were generated in the Monte Carlo calculation: $K_{\mu 3}^0$, K_{e3}^0, $K_{\pi 3}^0$, and $K_{\pi 2}^0$, with the branching ratios 0.268, 0.39, 0.126, and 2.07×10^{-3}, respectively.[16] The events were generated in the kaon center-of-mass system, with the charged decay products subsequently transformed to the laboratory system along the direction of the K_L^0. Table I shows the number of

generated events and the trigger efficiency for each mode.

The original set of form factor parameters used in generating K^0_{l3} Monte Carlo events were $\lambda_+ = 0.04$, $\lambda_- = -0.155$, and $\xi(0) = -2.0$. In the subsequent analysis, a Monte Carlo distribution with new form factors was generated by reweighting each event by the ratio of

$$\frac{|\mathfrak{M}(\text{new form factors})|^2}{|\mathfrak{M}(\text{original form factors})|^2} .$$

This procedure was much more economical, from the point of view of computer time used, than generating a completely new set of Monte Carlo events.

The $K^0_{\pi 3}$ events were generated according to the matrix element

$$|\mathfrak{M}|^2 = 1 + A(Q/m_K)Y + B(Q/m_K)^2Y^2, \qquad (19)$$

where $Y = 3T_0/Q - 1$, using the values $A = -5.20$ and $B = 4.64$.[17]

D. Pion decay and penetration

Pion decays, $\pi \to \mu\nu$, were included in the $K^0_{\mu 3}$ Monte Carlo events, using the pion decay length $c\tau = 780.2$ cm. The decay muons were generated isotropically in the pion center-of-mass system. Some 4.3% of all generated $K^0_{\mu 3}$ decays were followed by a pion decay before the pion reached the front surface of the lead wall.

K^0_L decays other than $K^0_{\mu 3}$ could satisfy the trigger when followed by a subsequent pion decay which resulted in a muon of sufficient energy to penetrate the lead wall. There were pion decays in 4.5% of all generated K^0_{e3} events, and in 10.2% of all generated $K^0_{\pi 3}$ events.

The problem of subtracting the background due to pion penetration of the muon filter is considerably more difficult. One needs to know not only the number of those events but also their relative density on the Dalitz plot when interpreted as $K^0_{\mu 3}$ events. It is difficult to answer the first question by Monte Carlo techniques, since in addition to pions penetrating without any interactions there could also be false muon signatures due to hadronic showers initiated by pions from K^0_L decay. Thus the total number of pion penetrations had to be determined directly from the data, as discussed in Sec. VI B.

To a reasonably good approximation, the question of the Dalitz-plot population by these events can be answered by Monte Carlo methods, since the reconstructed T_π and T_μ parameters are independent of the details of the penetration mechanism, and are merely a function of geometrical parameters measured before the lead wall. Thus in a sample of Monte Carlo K^0_L decays the strong interactions were effectively turned off, and the pions were allowed to trigger the appropriate B and C counters if they had enough energy to penetrate the muon filter. The penetrating pions were then treated as muons in the subsequent analysis.

TABLE I. Events generated by the Monte Carlo program and trigger efficiency for each decay mode.

Decay mode	No. generated	No. triggers	Trigger efficiency
$K^0_{\mu 3}$	2.13×10^7	4.0×10^6	18.8%
$K^0_{e 3}$	3.11×10^7	2.1×10^5	0.7%
$K^0_{\pi 3}$	1.00×10^7	1.5×10^5	1.5%
$K^0_{\pi 2}$	1.25×10^5	2.22×10^3	1.8%

E. Wire chamber and TOF data

Each charged decay product was traced through the magnetic field of the analyzing magnet from the decay vertex to the A counter bank. At the position of each of the 20 wire planes, the locations of the wires closest to the trajectories of the particles were recorded.

The TOF scheme employed for the Monte Carlo data was made to parallel that used in the experiment, where direct $v \simeq c$ muons from the production target were used to provide a reference time for all the timing counters, as described in paper I. For each charged track in the accepted Monte Carlo events, the TOF was computed along its path from the decay vertex to the A counter bank. The kaon TOF from the production target to the decay vertex and the light transit time in the counter were added to this time, while the TOF for a direct $v \simeq c$ muon from the target to the center of the A counter bank was subtracted. The TOF reading for each of the two phototubes on the corresponding A counter was then converted to an ADC reading, using the experimentally measured ADC sensitivity of 0.135 nsec/channel.

F. Muons

Since the identification of muons was a crucial part of the experiment, it was vital that the muon signal be reproduced in the Monte Carlo as realistically as possible. The two important features that had to be included in following the muon through the 8.7 interaction lengths of lead and paraffin which made up the muon filter were multiple scattering and energy loss. Since muons have no hadronic interactions, both these processes could be duplicated in the Monte Carlo to a

high degree of accuracy.

Only multiple Coulomb scattering was included for the muon, and the scattering angle was approximated by a Gaussian distribution of width

$$\theta = (0.021/P_\mu c)\sqrt{X_\tau}\,, \tag{20}$$

where P_μ is the momentum of the muon in GeV/c, and X_τ is the number of radiation lengths of material traversed by the muon. In tracing the muon trajectory through the lead and paraffin wall, the size of each step was adjusted as a function of the muon energy in order to keep the multiple scattering angle small, typically <50 mrad.

The only energy-loss mechanism which was considered for the muon as it traversed the muon filter was ionization energy loss. This loss was included as a function of the muon energy,[18] and the muon was considered to have stopped if its kinetic energy dropped below 1 MeV. Since the end-of-range effects were difficult to reproduce, they were not included in the Monte Carlo. However, such biases were later eliminated in the PASS-2 analysis by requiring that the total energy of the muon be >220 MeV at the position of the C counter.

The muon TOF was computed along each step in the wall and this was used in conjunction with the TOF at the A counter bank to compute TOF readings at the B and C counter banks for the muon, which were then converted to ADC readings.

G. Analysis programs

The Monte Carlo versions of the analysis programs PASS-1 and PASS-2 were identical to those used on experimental data except for one change in each program in order to introduce spark and TOF jitter, respectively. Details of these analysis programs have been given in paper I.

In PASS-1, each spark that was read off the Monte Carlo data tape was jittered about its true position in order to produce a Gaussian distribution with a width of 0.35 mm. This distribution reproduced the experimentally observed distribution of the distance of a spark along a track from the best-fit line through all the sparks making up that track.

It was more difficult to reproduce the TOF jitter since there were certain elements in the timing system which were not easily reproduced in the Monte Carlo calculation. First, there was the problem of fluctuations in the beam intensity and the quality of the beam steering, both of which affected the size of the CABLE pulse. The subsequent time slewing in the CABLE discriminator resulted in a time jitter for the START gate in the TOF system. Second, there was the problem of background, much of which was attributed to the neutron splash in the lead wall. Whenever there was a background track in a timing counter in addition to the charged track from the kaon decay, with both tracks falling within the timing gate, each phototube recorded the time of the first light which reached it, and this was not necessarily due to the decay product. This resulted in erroneous TOF measurements for the decay product, and sometimes an unphysical TOF measurement, if the reading should fall in the range where the event could have been interpreted as being associated with a decay from the previous or following beam buckets.

A study has shown that to a good approximation these problems were random in nature, and therefore could not have caused a systematic bias in the data. The measured kaon TOF was used only to decide which of two possible solutions for the K_L^0 momentum was the more probable, as discussed in Sec. VI C. For this purpose, it was sufficient to ask only that the Monte Carlo and experimental TOF distributions have the same shape, regardless of the details of how one arrived at that shape. Similarly, only the over-all shapes of the TOF distributions in the A, B, and C counter banks were relevant when the PASS-2 analysis program searched for muon candidates, as discussed in paper I.

We were able to obtain a satisfactory agreement between the Monte Carlo and the experimental TOF distributions by adding Gaussian errors of width 0.3 nsec to the A counters, and of width 0.4 nsec to the B and C counters for each event in the Monte Carlo version of PASS-2, and then folding in a common Gaussian jitter of width 0.25 nsec to account for the effects of CABLE slewing and neutron interactions.

The PASS-3 analysis program applied the final cuts and displayed numerous histograms, as well as storing the latter on disk for an over-all summary. It was identical for both the data and Monte Carlo distributions.

VI. DETERMINATION OF DALITZ-PLOT DENSITY

A. Event selection

The selection criteria used in choosing the events accepted for final analysis were dictated by the desire to obtain a sample of $K_{\mu 3}^0$ decays as pure as possible and at the same time one that could be faithfully reproduced by Monte-Carlo programs. We have used only those events in which both charged particles were detected on both sides of the magnet and in which the muon identification was unambiguous (category of events called 2 TRACK in paper I). There was one minor excep-

tion to the latter criterion. A small fraction of the data could be expected to correspond to the physical situation illustrated in Fig. 6, i.e., the pion, or one of its secondaries could penetrate up to the B bank and register a valid signal in one of the B counters. Because of the presence of this additional B counter, some of these events might be classified as AMBIGUOUS events, i.e., one where either track could be a muon since the single C counter could be associated with either track. Since it was not feasible to simulate this pion penetration in the Monte Carlo program, this category of events would be expected to be strongly suppressed in the Monte Carlo events. This indeed was the case, as this subsample made up 0.37% of the accepted events in real data, but only 0.09% (due to $\pi \to \mu\nu$ decay) in the Monte Carlo distribution. Even though this constitutes a very small fraction of the data, the discrepancy is important at the level of our statistical precision, since these events are biased in favor of high transverse momenta for the two charged tracks, and hence high T_π and T_μ on the Dalitz plot. Thus this subset of the AMBIGUOUS events was also included among the accepted events. The track giving the better "muon χ^2" was defined to be the muon.

The events meeting the criteria described above were then required to pass a number of cuts. These cuts and their motivation are described below:

(1) Decay vertex cut. The Z coordinate of the decay vertex was required to lie at least 40 cm downstream of the veto counter and 30 cm upstream of the T counter bank to eliminate possible counter interactions. Furthermore, the X and Y coordinates were required to be at least 2 cm inward from the edge of the nominal beam envelope.

(2) The two charged tracks were required to hit two distinct T counters and two distinct A counters. The former requirement was imposed to be consistent with the trigger, the latter to select events with valid TOF information.

(3) $|X_1 - X_2| \geq 7$ cm if Y_1 and Y_2 had the same sign, where X_i and Y_i refer to the X and Y coordinates of the two charged tracks at the T bank. This cut was imposed to avoid the possibility of having both charged tracks actually hitting the same T counter, with a δ ray from one of the particles triggering a neighboring counter. Because of tolerances allowed in the programs, different T counters could sometimes be assigned in this situation to the two charged tracks. This cut eliminated that possibility.

(4) $P_\pi \geq 1.15$ GeV/c. This cut eliminated low-energy pions which were more susceptible to nuclear absorption and also more likely to give very wide angle tracks in the rear chambers, for which PASS-1 was slightly inefficient.

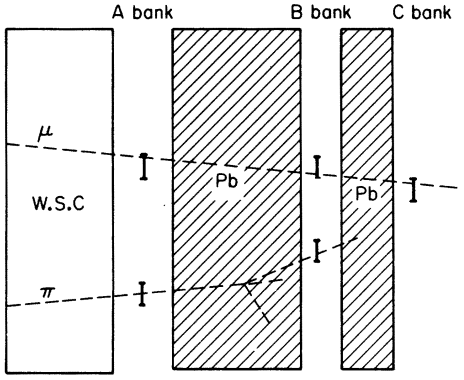

FIG. 6. A schematic diagram of an accepted AMBIGUOUS event. The B counter struck by the muon is too far away from the projected trajectory of the pion to be associated with it.

(5) The residual muon energy at the C bank, as calculated from track curvature and the amount of lead along its path, was required to be greater than 220 MeV. This eliminated a number of π penetrations and μ captures and/or decays at the very end of the lead wall.

(6) Events were eliminated if $-0.003 \leq P_0'^2 \leq 0.01$. This cut substantially reduced the contribution from $K^0_{3\pi}$ followed by π decay.

(7) $|\alpha_1 - \alpha_2| \geq 6$ mrad and $|\beta_1 - \beta_2| \geq 6$ mrad, where α and β refer to the X and Y direction cosines of the two charged tracks in the front chamber. For an angular separation smaller than this, the projections of the two tracks could coincide in one view with a resultant loss of accuracy difficult to duplicate in the Monte Carlo program.

(8) $Q \equiv p_\nu^\perp - p_\nu^* \leq 15$ MeV $- 0.03 p_\nu^*$, where p_ν^* is the center-of-mass neutrino momentum as determined from the π and μ four-vectors, and $p_\nu^\perp$ is the transverse component of the neutrino momentum in the laboratory system as obtained from the K_L^0 direction and π and μ momentum vectors. Q must clearly be negative for genuine $K^0_{\mu 3}$ events, in the absence of measurement errors. The cut chosen had a slight p_ν^* dependence to allow for a small variation of the experimental resolution as a function of p_ν^*.

(9) $m_{\pi\mu} \leq m_K$, where $m_{\pi\mu}$ is the invariant mass of the $\pi\mu$ system.

(10) $P_K \leq 14$ GeV/c. The momentum spectrum of the incident kaons was determined rather poorly above this value.

(11) $|\mathrm{TOF}_{\mathrm{measured}} - \mathrm{TOF}_{\mathrm{fit}}| \leq 0.6$ nsec.

(12) Events with more than one C counter were rejected. This cut was designed to reduce the number of events containing possible π penetra-

tions through the lead wall.

The fraction of events eliminated by each one of these cuts is listed in Table II. 34% of all the 2 TRACK events passed all of these cuts and entered the subsequent analysis.

B. Background corrections

In this section we consider the procedure used to eliminate or correct for any background events remaining in the sample after the cuts. Background sources greater than 0.1% are listed in Table III. These and other smaller background contributions are discussed below.

1. *Interactions in helium*

Some of the incident kaons or neutrons interacted with the helium nuclei in the decay volume, resulting in the production of a certain number of π's and K's. If one of the secondaries then decayed in flight, the trigger could be satisfied and the reconstructed event might satisfy our selection criteria.

To investigate this source of background, a series of short runs were made with a 1-in.-thick carbon slab, large enough to intercept the entire beam envelope, placed at various positions along the beam axis in the decay volume. The mass of the carbon block was 29 times larger than the total mass of the helium. Allowing for the difference in cross section (assuming an $A^{2/3}$ dependence), and the different K_L^0 fluxes corresponding to the carbon and data runs, we estimate that the total number of carbon interactions in the carbon run amounted to about 67% of the total number of helium interactions in the data sample under consideration.

Figure 7 displays the vertex position of the events taken during the carbon run. The abscissa is chosen in such a way as to compensate for the decreasing precision in the Z determination of the decay vertex as the event occurs further upstream. The graph is compatible with no interaction contamination. More specifically, we can place an upper limit of 10^{-4} of the accepted data as being due to interactions in helium. No correction was deemed necessary.

TABLE II. Effect of cuts on primary data. Cuts are outlined in Sec. VI A.

Cut no.	Fraction of events eliminated
1	9.0%
2(T counters)	4.0%
2(A counters)	7.4%
3	8.0%
4	8.8%
5	10.2%
6	2.2%
7	4.7%
8	1.2%
9	0.9%
10	0.2%
11	6.2%
12	3.8%

2. π-*decay background*

A 3-GeV pion resulting from a K_L^0 decay in the middle of the decay volume had a 6% probability of decaying before it reached the lead wall. Thus the other decay modes of K_L^0 which contain pions were a potentially serious source of background. The subtraction of this background can, however, be performed with high precision by a Monte Carlo method.

TABLE III. Sources of background greater than 0.1%.

Kind of background	Magnitude of background subtraction (%)
Diffraction scattering in air	0.70
Diffraction scattering in veto counter	0.18
$K_L^0 \to \pi^{\mp} e^{\pm} \nu$ followed by $\pi \to \mu \nu$	2.62
$K_L^0 \to \pi^+ \pi^- \pi^0$ followed by $\pi \to \mu \nu$	1.43
$K_L^0 \to \pi^+ \pi^-$ followed by $\pi \to \mu \nu$	0.05
$K_L^0 \to \pi^{\mp} \mu^{\pm} \nu \gamma$ ($E_\gamma > 2$ MeV)	0.94
$K_L^0 \to \pi^{\mp} e^{\pm} \nu$ followed by π penetration	0.36
$K_L^0 \to \pi^+ \pi^- \pi^0$ followed by π penetration	0.10
$K_L^0 \to \pi^{\mp} \mu^{\pm} \nu$ followed by π penetration (μ does not have enough energy to reach the C counter bank)	0.25

We have corrected for the background due to $\pi \to \mu\nu$ decays following each of the following four decay modes:

(a) $K_L^0 \to \pi^\pm \mu^\mp \nu$,
(b) $\to \pi^\pm e^\mp \nu$,
(c) $\to \pi^+\pi^-\pi^0$,
(d) $\to \pi^+\pi^-$.

The appropriate number of $K_{\mu 3}^0$ events followed by $\pi \to \mu\nu$ decay have been incorporated into the Monte Carlo program (see Sec. V D) which generated a large number of $K_L^0 \to \pi\mu\nu$ events for the purpose of calculating the detection efficiency. Thus no additional treatment of this contamination was necessary for mode (a).

The fraction of accepted $K_{\mu 3}^0$ events in which the μ trigger was generated by the muon from π decay was calculated to be 0.67%. Note that the events with two muons detected at the C bank, both the primary one and the secondary resulting from $\pi \to \mu\nu$ decay, would not be included in the final data sample, as they would be classified as 2 MUON events.

The contamination introduced by $\pi \to \mu\nu$ decays following the last three decay modes (b)–(d) was studied by Monte Carlo methods. Appropriate samples of events representing these decay modes and followed by π decay were generated according to the proper kaon momentum distribution and appropriate matrix elements. These events were subsequently processed through all the standard $K_{\mu 3}^0$ analysis programs, and the events remaining after all the cuts have been applied were then subtracted from the true data sample. The subtraction for the decay modes (b)–(d) amounted to 4.1% of the total data.

3. π penetration

Another potential source of contamination was pion penetration, i.e., the possibility that a pion either would not interact at all in going through the lead wall, or that one of the secondaries (or one of the higher generation particles) from the pion interaction could penetrate all the way to the C counter bank, resulting in a false muon signature. As the total amount of lead and paraffin corresponded to 8.7 interaction lengths, the probability of the former is less than 10^{-3}; it is more difficult, however, to estimate the effect of the much more complicated nuclear shower mechanism. Fortunately, there are two independent ways to measure this contamination experimentally in the actual data.

First, we can compare the expected and observed number of 2μ events. Any pion penetration will appear as an excess of 2μ events in the data. The empirical numbers for the ratio of 2μ events passing all cuts (except μ TRACK and $1C$ requirements) to accepted events are

$(2.62 \pm 0.05) \times 10^{-2}$ for Monte Carlo,

$(3.00 \pm 0.05) \times 10^{-2}$ for data.

The difference is $(0.38 \pm 0.07) \times 10^{-2}$, or $(14 \pm 3)\%$ of the 2μ events resulting from $K_{\mu 3}^0$ decays followed by a $\pi \to \mu\nu$ decay.

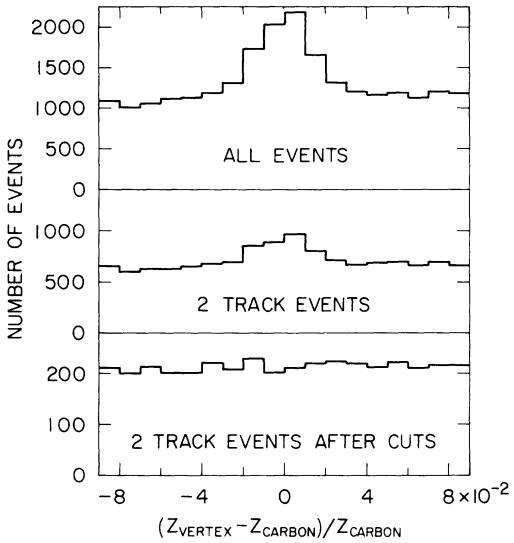

FIG. 7. Vertex distribution of the events in the carbon run.

An independent test consists of examining $P_0'^2$ distribution for the events passing all the cuts except the $P_0'^2$ cut. Any excess in the data near $P_0'^2 = 0$, over that expected from $K_{\mu 3}^0$ decays and other K_L^0 decays followed by $\pi \to \mu\nu$ decay, would be an indication of pion penetration from the $K_{\pi 3}^0$ decay mode. We find a slight excess (see Fig. 14, paper I), which corresponds to $(15 \pm 4)\%$ of the events due to $K_{3\pi}^0$ followed by $\pi \to \mu\nu$ decay. Thus we draw the conclusion that

$$\frac{\text{number of } \mu \text{ signatures due to } \pi \text{ penetration}}{\text{number of } \mu \text{ signatures due to } \pi \to \mu\nu \text{ decay}} = 0.14 \pm 0.03.$$

The pion penetration background was subtracted by the same Monte Carlo technique as used for π decays, except that now an appropriate fraction of the pions were allowed to have a μ signature. The size of this correction is indicated in Table III. Because this background was small, and its dependence on pion momentum relatively weak, the only dependence of the pion penetration probability on the pion laboratory energy included in the correction was the requirement that the pion range should be sufficient to penetrate through the lead wall.

4. Diffraction scattering in air and the veto counter

Between the γ-ray lead absorber and the decay volume, the K_L^0 passed through about 65 m of air and a 6.4-mm-thick veto counter. There was thus the possibility that a K_L^0 could diffractively scatter in the air or the veto counter and then subsequently decay in the decay volume. For a small-angle diffraction scattering on a carbon atom, the veto counter probably would not have been triggered by the recoiling nucleus. The K_L^0 direction as determined from the decay vertex and the target position would not correspond to the actual K_L^0 direction for these diffractively scattered events.

We have calculated the effect of this background by Monte Carlo, allowing the incident K_L^0's to scatter diffractively all along its flight path, and then processing through our analysis programs those events which decayed in the decay volume. For lack of good experimental information, we have used for the total cross sections the geometrical collision lengths in air and scintillator of 536.1 m and 52 cm, respectively.[19] We have taken the diffraction scattering cross section to be $\frac{1}{3}$ of the total cross section, and assumed a scattering t dependence of the form e^{-50t} and independent of energy.

Clearly, the uncertainty in the parameters is such that this calculation cannot be taken too literally. It should, however, be accurate to better than a factor of 2, and since this correction turns out to be quite small (see Table III), we feel confident that no significant errors were introduced by this potential source of background.

5. Radiative corrections

As there are two charged particles in the final state, radiative corrections for K_{l3}^0 decays are substantially larger than those for K_{l3}^+ decays. The order-α radiative corrections to K_{l3}^0 decay are shown in Fig. 8. Several recent K_{l3}^0 experiments have had a statistical accuracy which warrants the inclusion of radiative corrections, but these have not always been applied. In those cases where corrections have been made, the results of Ginsberg[20] have been applied to the extracted Dalitz-plot distribution.

Since the Ginsberg calculation assumes that only the pion and lepton are detected by the apparatus, it integrates over all photon four-momenta in calculating the bremsstrahlung contribution [Figs. 8(g) and 8(h)], and assumes that the reconstructed T_π and T_μ correspond to the actual values. Ginsberg's radiative corrections are, therefore, applicable only to an experiment which meets two rather stringent requirements:

(1) The detection apparatus must integrate over all photon four-momenta with 100% efficiency. This is not, in general, the case. For example, a bremsstrahlung event in which the pion and muon center-of-mass energies are within the Dalitz-plot boundary, but which includes a reasonably high energy photon, may fail specific geometrical or kinematic cuts. Ginsberg's calculation assumes that all such bremsstrahlung events will be detected.

(2) The experiment must determine the value of E_π^* and E_l^* in the kaon rest frame without kinematical assumptions. If this is not the case, then $K \to \pi l \nu \gamma$ events in which only the pion and lepton are detected in the laboratory may be placed on the K_{l3} Dalitz plot, even if the pion and lepton have true center-of-mass energies which would place them outside the K_{l3} Dalitz-plot boundary (i.e., events which belong to $R_{\rm IV}$ but not $R_{\rm III}$, in Ginsberg's parlance). This is so because the event will perforce be placed on the Dalitz plot using three-body kinematics. Ginsberg explicitly assumes that such bremsstrahlung events do not contribute to the K_{l3} Dalitz plot. Bremsstrahlung events in which the pion and muon center-of-mass energies are actually within the Dalitz-plot boundary may also be moved substantially from their true position by the assumption of three-body kinematics.

The degree to which a particular experiment will fail to approximate these ideal conditions will depend, of course, on specifics of the apparatus, the momentum spectrum of incident kaons, and the method of resolution of the quadratic kinematic ambiguity. We know of no K_{l3} decay experiments which satisfy both requirements, however, and therefore we know of no experiment to which the Ginsberg corrections (or any other published radiative corrections)[21] are directly applicable.

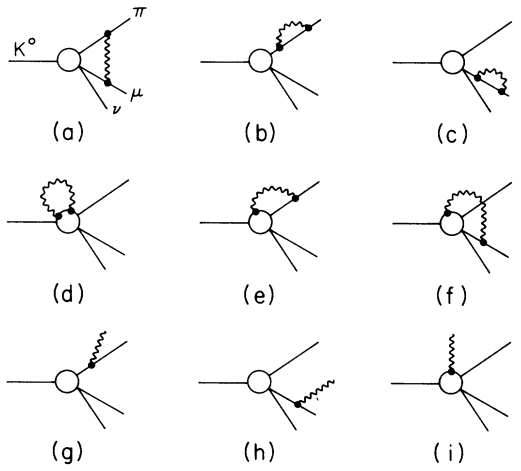

FIG. 8. Order-α radiative corrections to K_{l3}^0 decay.

We describe below the procedure we have followed in making radiative corrections to the present experiment. In order to include our experimental apparatus when making the bremsstrahlung corrections, we have divided the order-α diagrams into three parts:

(1) virtual diagrams [Figs. 8(a)–8(c)], which have no external photons,

(2) low-energy bremsstrahlung, in which the external photon energy is so small that the resulting change in the center-of-mass energy of the charged particle was less than the resolution of the apparatus, and

(3) high-energy bremsstrahlung, from the resolution of the apparatus to the kinematic limit.

Structure-dependent order-α radiative corrections [Figs. 8(d)–8(f), and 8(i)] have not been included, as they are model-dependent and no calculation of their contribution is known to us. Their contributions, however, are expected to be small.

Processes (1) and (2) were treated as multiplicative corrections and folded into the detection efficiency, while the correction for (3) was treated as a background subtraction.

The virtual contribution was calculated using the Ginsberg formulas, modified so as to remove the restriction to constant form factors. A small photon mass term, $\ln(m_\mu/\lambda)$, where λ denotes the photon mass, was included to cut off the logarithmic infrared divergence.

The low-energy bremsstrahlung contribution was calculated by Monte Carlo techniques, using the $K_L^0 \to \pi\mu\nu\gamma$ matrix element of Fearing, Fischbach, and Smith.[22] The photons were given a mass λ, and were required to have energy $E_\gamma^* < 2$ MeV. The photon mass λ was varied over four orders of magnitude to verify that the logarithmic divergences canceled exactly in the sum of virtual and low-energy bremsstrahlung contributions.

The high-energy bremsstrahlung contribution was calculated using a Monte Carlo technique by generating four-body $K_L^0 \to \pi\mu\nu\gamma$ decays with $E_\gamma^* > 2$ MeV, also according to the matrix element of Fearing, Fischbach, and Smith. An ultraviolet cutoff of one proton mass was used. These events were then processed through the analysis programs, in the same way as all other small contamination corrections.

Figure 9 represents a comparison of the $K_{\mu 3}^0$ radiative corrections as a function of the Dalitz-plot position, with and without the effect of the apparatus. Percentage corrections are shown in 10 $\times$ 10 MeV bins on the Dalitz plot for clarity, although in the analysis 5×5 MeV binning was used. The upper number in each bin is the percentage radiative correction obtained by integrating over the photon four-momentum numerically, without taking into account the detection apparatus or the effect of subsequent cuts in the analysis. The lower number in each bin is the percentage radiative correction (1)+(2)+(3) obtained when the integration is performed by Monte Carlo, including the effect of apparatus geometry and kinematic cuts. The lower numbers differ considerably from the upper, reflecting the inefficiency of the apparatus for high-energy bremsstrahlung events; this loss is approximately constant across the Dalitz plot.

6. *Accidentals*

The poor duty cycle of SLAC might have caused some accidentals to simulate real events. Specifically, we had to consider three kinds of accidentals:

(1) accidental B and C counter triggers which might be associated with a track from a genuine K_L^0 decay that was not a $K_{\mu 3}^0$ decay, resulting in an accidental muon;

(2) two uncorrelated tracks which verticized accidentally in the decay volume;

(3) a whole track which might be accidentally reconstructed from two uncorrelated segments, one upstream and one downstream of the magnet.

The first category of accidentals would be included in the pion penetrations, and thus to a good approximation have been accounted for in the correction for penetrations. Since this correction was relatively small, no further correction was considered necessary.

The amount of contamination due to the second mechanism was investigated by attempting to verticize the pion from event N with the muon from event $N+1$, and then subjecting the resulting "$K_{\mu 3}^0$ decay" to standard cuts. The total number of such false events was found to be $\sim 4 \times 10^{-4}$ of the total sample. The actual number of accidentals is probably a factor of 10 lower, since only about 10% of the events had additional "in time" tracks. In view of this very low contamination, no correction was applied.

The third mechanism can be estimated to be even less important than the second one, since the matching criteria for the upstream and downstream portions of the track, as described in paper I, involved three independent constraints, and were much more stringent than the requirement for a decay vertex. Again, no correction was deemed necessary.

7. *Other muonic decays*

Of the other possible K_L^0 decays involving muons,

$$\begin{aligned} K_L^0 &\to \pi^\mp \pi^0 \mu^\pm \nu\,, \\ &\to \mu^+ \mu^- \gamma\,, \\ &\to \mu^+ \mu^-\,, \end{aligned} \tag{21}$$

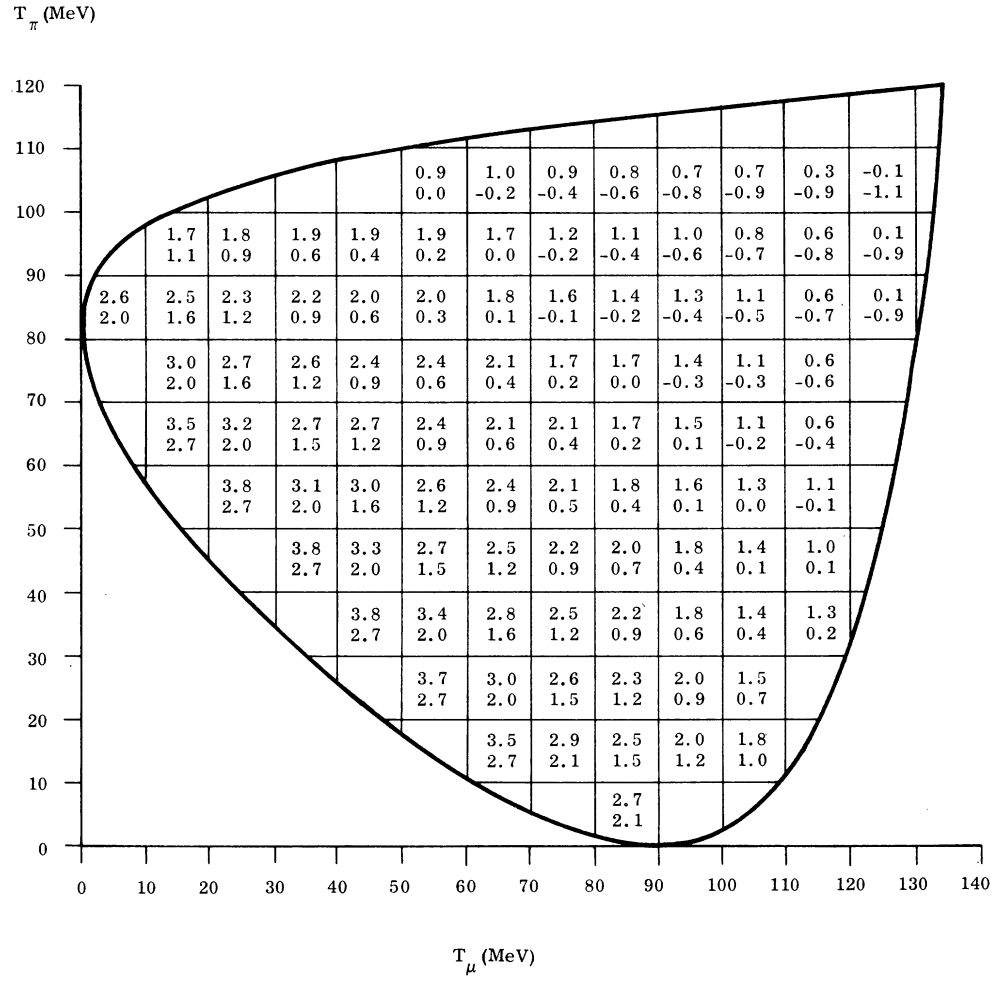

FIG. 9. Comparison of percentage radiative corrections across the Dalitz plot in 10×10 MeV bins for "ideal" apparatus (upper numbers in each box; average = 2.4%) and for the apparatus and K_L^0 spectrum of the present experiment (lower numbers; average = 0.9%).

only the first one might occur at a level to merit consideration. The events from this decay mode could potentially be dangerous, since they tend to populate a limited region of the Dalitz plot because of the low Q value of this decay. This decay has not as yet been observed, but one can make a crude estimate based on its charged K counterpart. The branching ratio for $K^+ \to \pi^+\pi^-\mu^+\nu$ is reported to be $(9 \pm 4) \times 10^{-6}$.[19] Multiplying by the ratio of K_L^0/K^+ lifetimes, we estimate the $K_{\mu 4}^0$ decay to be suppressed by roughly 10^4 with respect to $K_{\mu 3}^0$. Furthermore, the probability that a $K_{\mu 4}^0$ event would be detected by the apparatus and pass all the $K_{\mu 3}^0$ cuts described previously is about a factor of 3 lower than for $K_{\mu 3}^0$. Thus the background is estimated to be $\approx 3 \times 10^{-5}$ and can be neglected.

C. Quadratic ambiguity

Since we measure the momentum vectors of the two charged decay products quite well, the invariant mass of the $\pi\mu$ system is accurately determined:

$$m_{\pi\mu}^2 = (p_\mu + p_\pi)^2 , \tag{22}$$

where p_π and p_μ are the pion and muon four-momenta. Thus the neutrino center-of-mass momentum p_ν^* is also accurately determined:

$$p_\nu^* = \frac{m_K^2 - m_{\pi\mu}^2}{2m_K} . \tag{23}$$

Furthermore, once the decay vertex is reconstructed, the direction of the K_L^0 is known to a high precision. Thus, by conservation of momen-

tum and Lorentz invariance, the component of the neutrino momentum transverse to the K_L^0 direction $p_\nu^\perp$, is given by

$$p_\nu^\perp = -(p_\pi^\perp + p_\mu^\perp) , \tag{24}$$

where $p_\pi^\perp$ and $p_\mu^\perp$ are the transverse momenta of the pion and muon relative to the K_L^0 direction, respectively. The longitudinal component of the neutrino center-of-mass momentum is thus determined up to a sign:

$$p_\nu^\parallel = \pm (p_\nu^{*2} - p_\nu^{\perp 2})^{1/2} . \tag{25}$$

Alternatively, looking at the problem entirely in the laboratory system, we can say that the conservation of energy and momentum in the decay $K_L^0 \to \pi\mu\nu$ provides us with four constraints. If the TOF measurement providing the K_L^0 energy information is ignored, then we are missing four quantities: the total momentum of the K_L^0, the total momentum of the neutrino, and the two parameters describing the neutrino direction. Thus we can solve for the energy of the K_L^0, or for $\gamma \equiv E_K/m_K$:

$$\gamma = \frac{E_{\pi\mu}(m_K - p_\nu^*) \pm p_\nu^\parallel p_{\pi\mu}^\parallel}{E_{\pi\mu}^2 - p_{\pi\mu}^{\parallel 2}} , \tag{26}$$

where $E_{\pi\mu}$ and $p_{\pi\mu}^\parallel$ are the energy and the longitudinal momentum of the $\pi\mu$ system. The sign ambiguity corresponds to the ambiguity in the direction of the neutrino center-of-mass longitudinal momentum, the plus sign corresponding to forward emission of the neutrino. Since the center-of-mass kinetic energies of the pion and muon, T_π and T_μ, and thus the position on the Dalitz plot, depend directly on the Lorentz transformation parameters used, we have a twofold ambiguity in the location of each event on the Dalitz plot.

We might mention here in passing that due to measurement errors, situations arose where no real solutions exist. This occurred when $m_{\pi\mu} > m_K$ or $p_\nu^\perp > p_\nu^*$, the latter case causing the radicand in the expression for $p_\nu^\parallel$ to be negative. The

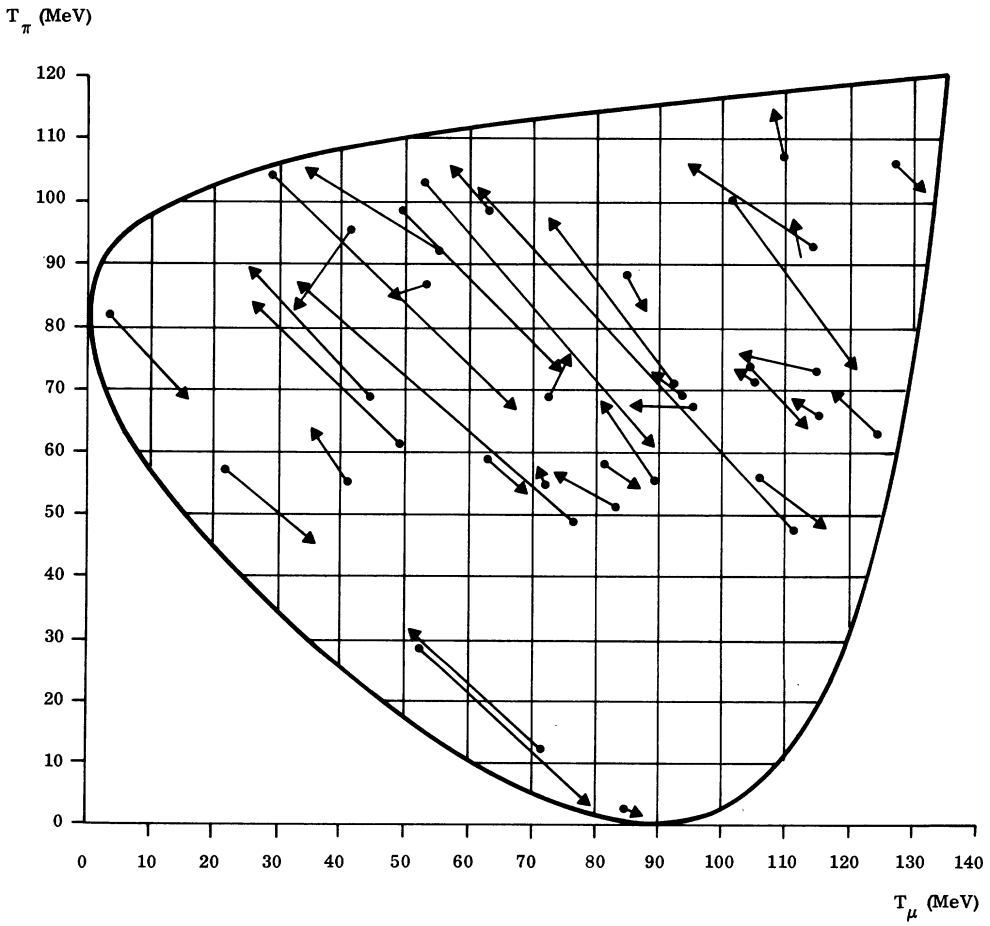

FIG. 10. The displacement due to the choice of a wrong solution for 40 random Monte Carlo events. The arrows point from the true (T_π, T_μ) point to the reconstructed (T_π, T_μ) point.

small fraction of events with $m_{\pi\mu} > m_K$ was eliminated from the data (Sec. VI A), but some of the events which barely failed the $p_\nu^\perp > p_\nu^*$ criterion (cut 8 in Sec. VI A) were included in the final sample. The radicand for such events was set equal to zero.

To resolve the quadratic ambiguity, we have utilized both the momentum spectrum of the K_L^0 beam and the TOF information. Using the Monte Carlo generated events, we have first generated a function $P(P_K, Z)$ giving the *a priori* probability that a K_L^0 of momentum P_K would give a detected $\pi\mu\nu$ decay if it decayed at a distance Z from center of the spectrometer magnet. Then for each event we calculated the ratio R given by

$$R = \frac{P(P_K^1, Z)e^{-(t_1 - t_m)^2/2\sigma^2}}{P(P_K^2, Z)e^{-(t_2 - t_m)^2/2\sigma^2}} , \tag{27}$$

where P_K^1 and P_K^2 are the fitted K_L^0 momenta, t_m is the measured TOF, and t_1 and t_2 are the fitted TOFs corresponding to solution 1 and solution 2, respectively. The quantity σ corresponding to the TOF error was taken to be 0.36 nsec. Solution 1 was chosen if $R > 1$. Since the identical procedure was followed for both Monte Carlo and data, the choice of the wrong solution only tends to dilute the statistical significance of the data, but does not introduce any bias provided that the Monte Carlo faithfully reproduces the actual experiment.

Even though the fraction of events with wrong solutions, defined as those events which end up in the wrong 5×5 MeV bin due to the choice of the incorrect solution for γ, was relatively high (17.6%), on the whole there was very little net movement across the Dalitz plot. Furthermore, the typical displacement from the true position was rather small. These points are illustrated in Figs. 10–12, which show the movement due to the choice of the wrong solution for 40 random Monte Carlo events, the net inflow or outflow from each bin due to the choice of the wrong solution, and the distribution of the shift in T_π for these events.

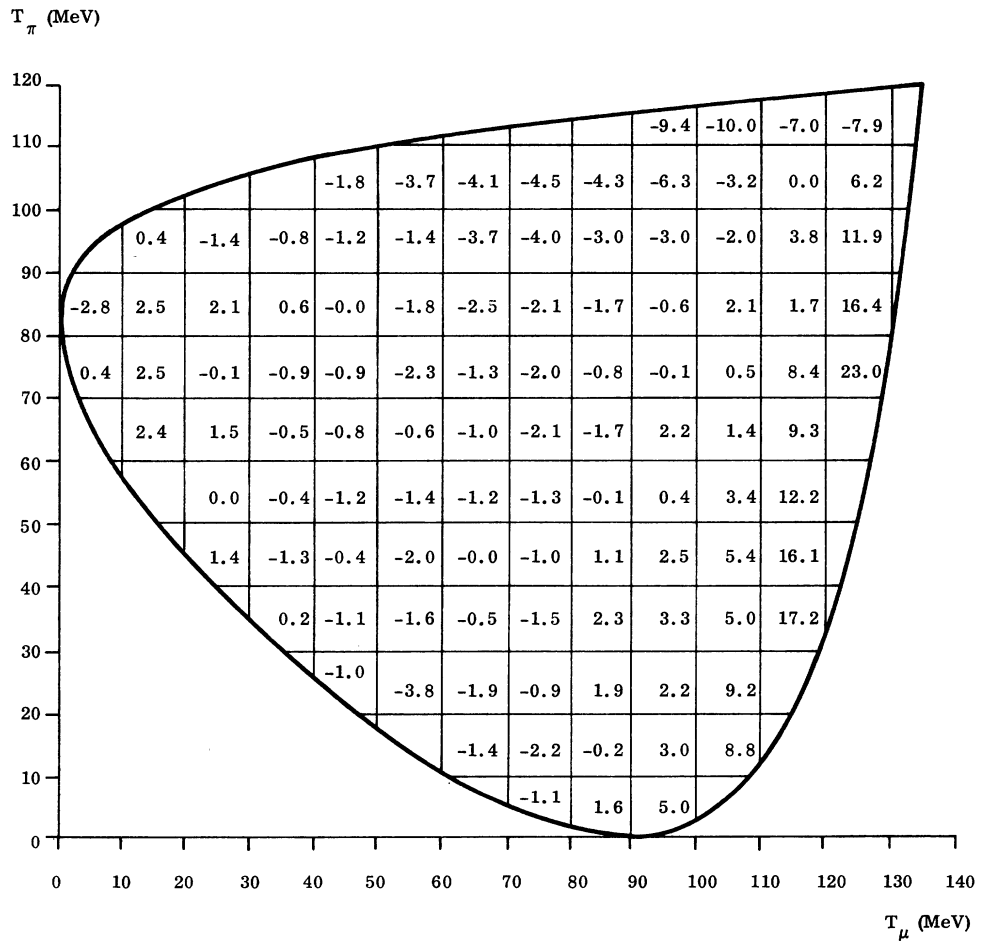

FIG. 11. The net percentage change in Dalitz-plot population due to "wrong solutions." The results are displayed in 10×10 MeV bins for clarity.

D. Calculation of the population in each bin

The number of events N_i corrected for background in a given bin i was given by

$$N_i = M_i - \sum_{j=1}^{9} k_j m_{ji} \ , \tag{28}$$

where M_i = the total number of accepted events in bin i, m_{ji} = the number of events of background j in bin i, and k_j = a factor of the order of unity to obtain proper normalization for each background. The nine types of background considered and their total magnitude are listed in Table III.

The raw number of events then had to be corrected for the detection efficiency. The efficiency in any one bin i was given by

$$\epsilon_i = d_i/G_i \ , \tag{29}$$

where d_i is the number of accepted Monte Carlo events that end up in bin i, and G_i is the number of generated Monte Carlo events in bin i. We stress that the contribution to d_i can also come from events generated into bins other than the bin i, which, owing to measurement errors or the choice of the wrong solution, migrated to bin i. The efficiency as a function of position on the Dalitz plot is displayed in Fig. 13.

The final corrected number of events n_i is then given by

$$n_i = N_i/\epsilon_i r_i \ , \tag{30}$$

where r_i is the enhancement in the bin i due to the virtual radiative corrections and low-energy (<2 MeV) inner bremsstrahlung. The error δn_i is given by

$$\delta n_i = n_i \left(\frac{M_i + \sum_{j=1}^{9} k_j^2 m_{ji}}{N_i^2} + \frac{1}{d_i} \right)^{1/2} . \tag{31}$$

Error correlations between various bins due to movement of events from one bin to another can be safely ignored. It is the distribution $(n_i \pm \delta n_i)$ which is subsequently fitted to a theoretical spectrum.

E. Data

The final sample of data consisted of two subsets: 754 000 events and 836 000 events, collected several months apart. These events are shown in their reconstructed position on the Dalitz plot in Fig. 14. For clarity 10×10 MeV bins are used in the figure. The two subsets differed slightly in the incident K_L^0 momentum spectrum, precision of TOF information, and beam collimation. The parameters of the Monte Carlo sample, which consisted of 800 000 triggers passing the $K_{\mu 3}^0$ cuts, were adjusted accordingly for each subset.

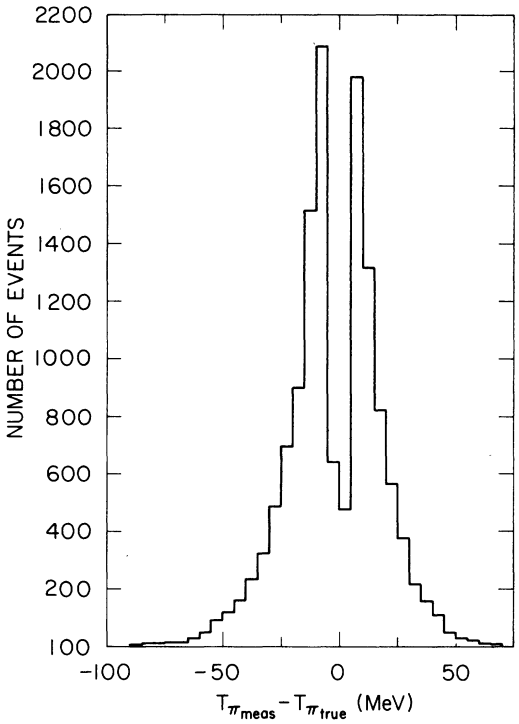

FIG. 12. The shift in the pion center-of-mass energy for "wrong solution" events as determined from the Monte Carlo.

VII. FITTING PROCEDURE AND RESULTS

The fitting of the data sample to theoretical expressions was done in 5×5 MeV bins; only those bins lying entirely within the Dalitz-plot boundary were included in the analysis. Four types of fits were made to the data:

(1) an "unparametrized" fit using f_+ and f_0 form factors, and fitting each of the 22 t bins independently;

(2) an unparametrized fit using f_+ and ξ form factors, and fitting each of the 22 t bins independently;

(3) a "2-parameter" fit in which the entire Dalitz plot was fitted simultaneously using the parametrization

$$f_+(t) = f_+(0)\left(1 + \lambda_+ \frac{t}{m_\pi^2}\right) \ , \qquad f_0(t) = f_0(0)\left(1 + \lambda_0 \frac{t}{m_\pi^2}\right) \ ; \tag{32}$$

(4) a 2-parameter fit in which the entire Dalitz plot was fitted simultaneously using the parametrization

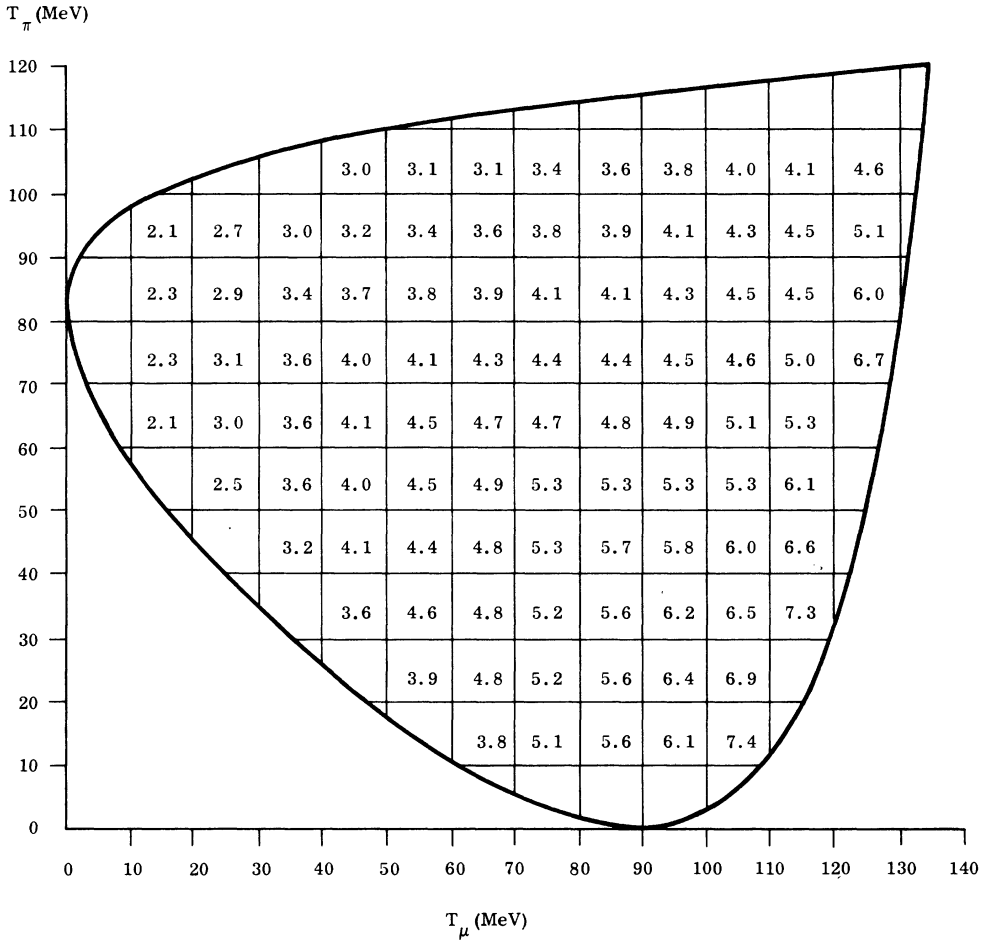

FIG. 13. Acceptance efficiency (ϵ) after all cuts in percent as a function of Dalitz-plot position as calculated by the Monte Carlo program. Again 10×10 MeV bins are chosen for clarity.

$$f_+(t)=f_+(0)\left(1+\lambda_+\frac{t}{m_\pi{}^2}\right),$$
$$\xi(t)=\frac{m_K{}^2-m_\pi{}^2}{m_\pi{}^2}\,\frac{(\lambda_0-\lambda_+)}{(1+\lambda_+ t/m_\pi{}^2)}\,. \tag{33}$$

In these last two fits, $f_+(0)\equiv f_0(0)\equiv 1$.

The 22 values of the form factors at different t derived from the first two procedures were then fitted with a polynomial to determine their t dependence. Both f_+ and f_0 were found to be satisfactorily described by a linear t dependence, while ξ was found to be consistent with having a constant value over the range of t examined in this experiment. The results of the four fits are tabulated in Table IV. Values of f_+, f_0, and ξ as a function of t as obtained from fits (1) and (2) are displayed in Fig. 15. The residuals of the 2-parameter fit to λ_+ and λ_0 are shown in Fig. 16. The errors shown in Table IV and Fig. 15 are statistical only. A detailed discussion of our estimation of systematic errors will be presented in Sec. VIII.

The slope of the f_+ form factor found in this experiment supports the hypothesis that $f_+(t)$ obeys an unsubtracted dispersion relation, and that the dispersion integral is saturated by the $K^*(890)$ pole. A 2-parameter fit in which the mass of a single 1^- pole describes the t dependence of f_+ yields $m_*(1^-)=870\pm17$ MeV, in excellent agreement with the $K^*(890)$ dominance prediction.

The slope of the f_0 form factor found in this experiment is in excellent agreement with the Dashen-Weinstein relation (if we allow a linear extrapolation to $t=m_K{}^2+m_\pi{}^2$), supporting the view that the effects of SU(3)$\otimes$SU(3) breaking in the strong interactions are small enough so that a perturbative treatment is valid. The extrapolated value of f_0 at $t=m_K{}^2-m_\pi{}^2$ is 1.22 ± 0.04, in excellent agreement with the modified Callan-Treiman relation. Thus, these experimental results also support the

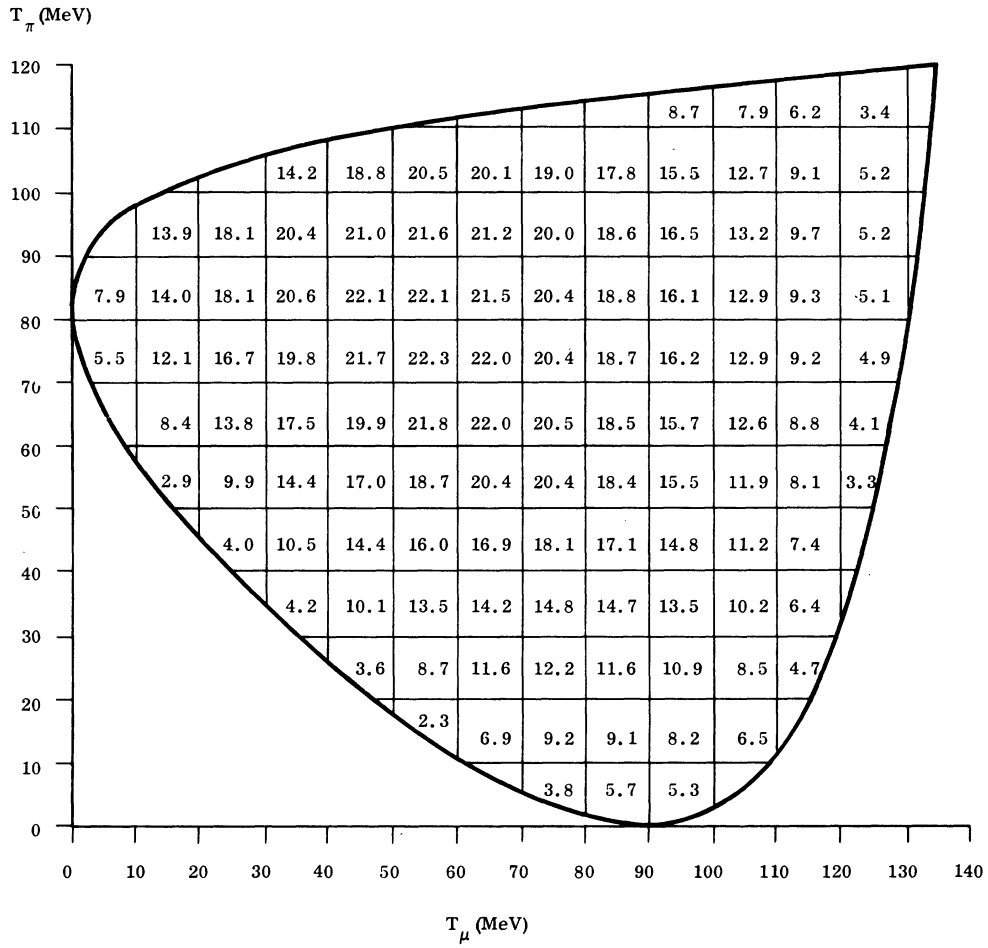

FIG. 14. Number of events after background subtraction (in thousands) as a function of their reconstructed position on the Dalitz plot.

view that SU(2) ⊗ SU(2) is a good symmetry of the strong interactions, by bearing out the PCAC prediction.

In Table V we summarize the results of several other parametrized fits to the data. The K^* pole fit has already been discussed. A fit requiring both 1^- and 0^+ poles gives $m_*(1^-) = 867 \pm 18$ MeV and $m_*(0^+) = 1109 \pm 42$ MeV; our data are therefore also in agreement with the requirement that $f_0(t)$ obey an unsubtracted dispersion relation, and the use of the broad $K\pi$ enhancement at 1200–1400 MeV as the 0^+ pole.

Finally, we have performed a fit in which f_+ and f_0 were allowed to have linear t dependence and included a constant tensor amplitude f_T. This fit provides a very stringent limit on any possible tensor contribution to the matrix element: $|f_T| < 0.016 f_+(0)$ at the 95% confidence level. Because of the "induced scalar" term resulting from the vector form factors, the $K^0_{\mu 3}$ Dalitz-plot analysis is unable to extract any information on a possible scalar amplitude.

TABLE IV. Results of the four primary fits to the $K^0_{\mu 3}$ Dalitz plot. Errors shown are statistical only.

	Over-all χ^2	Degrees of freedom	λ_+	λ_0	ξ
Unparametrized fit	329	357	0.033 ± 0.004	0.013 ± 0.005	0.00 ± 0.04
2-parameter fit	396	398	0.030 ± 0.0015	0.019 ± 0.0014	-0.11 ± 0.02

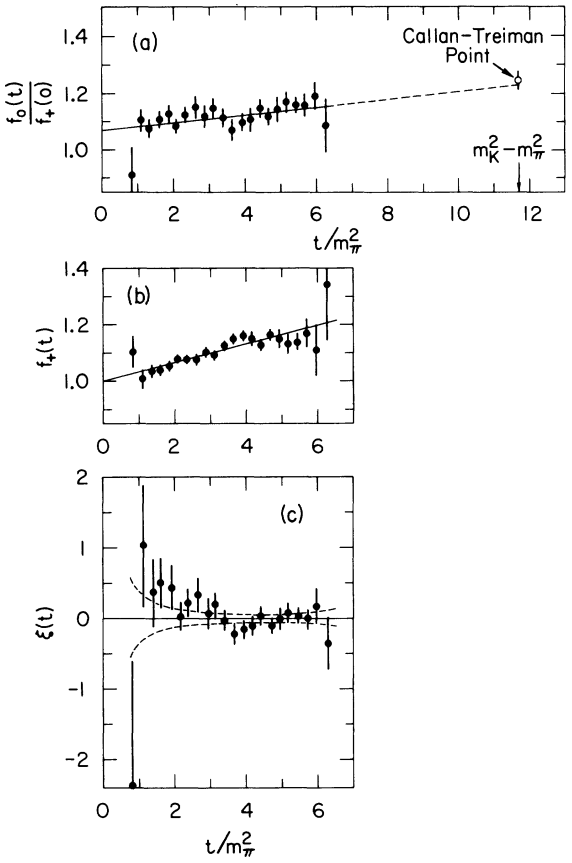

FIG. 15. Results of the "parameter-independent" fits. (a) f_0 as a function of t, (b) f_+ as a function of t, and (c) ξ as a function of t. The straight lines in (a) and (b) represent the best linear fit to the data; the dashed line in (c) is our best estimate of systematic errors. The Callan-Treiman point was not included in the fit.

The results obtained depend slightly on the values of the form factors used as input to the Monte Carlo calculation, since the calculated efficiency is weakly dependent on these parameters, owing to the possibility of events migrating from one bin to another as a result of the fitting procedure. Thus, strictly speaking, when evaluating the χ^2 at any point characterized by λ_+ and λ_0 (or ξ), one should use corresponding parameters in the Monte Carlo calculation to evaluate the efficiency. As this procedure would consume a prohibitive amount of computer time, we have adopted an iterative procedure, reweighting the Monte Carlo events to correspond to the values of λ_+ and ξ yielded by the data after each fit. The final parameters used in the Monte Carlo calculation agreed with the eventual values given by the fit. The rapid convergence of this procedure is illustrated in Table VI, which confirms that the results of the fit do not have a strong dependence on the parameters used in the Monte Carlo calculation. We see that the main effect of using incorrect parameters in the Monte Carlo calculation would be to pull the resultant fit values slightly towards the parameters used. Since the values of λ_+ and λ_0 used in the final Monte Carlo calculation agreed with the values obtained in the final fit, no systematic error was introduced by this procedure. The net result of this procedure, however, was to underestimate the statistical error of λ_+ by about 7%, and λ_0 by 17%.

It is well known that in an unparametrized fit to f_+ and ξ, the extracted values of the form factors at a given t are strongly correlated, especially at low values of t. The extracted values of f_+ and f_0 at a

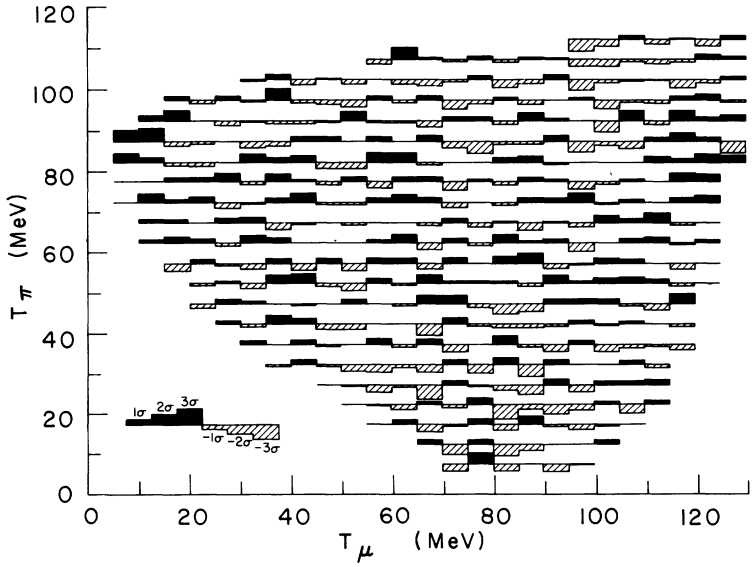

FIG. 16. Residuals of the 2-parameter (λ_+, λ_0) fit. The results are displayed in 5×5 MeV bins.

TABLE V. Results of several fits using other parametrizations of the form factors. Errors shown are statistical only.

Type of fit	Result
1^- pole, λ_0	$m_*(1^-) = 870 \pm 17$ MeV $\lambda_0 = 0.018 \pm 0.0015$
1^- pole, 0^+ pole	$m_*(1^-) = 867 \pm 18$ MeV $m_*(0^+) = 1109 \pm 42$ MeV
Inclusion of constant tensor amplitude	$\lambda_+ = 0.030 \pm 0.0016$ $\lambda_0 = 0.019 \pm 0.0015$ $f_T/f_+(0) = -0.001 \pm 0.008$

given t are also strongly correlated. This is illustrated in Fig. 17, where we show error ellipses for several different t values. In addition to the correlation of the parameters, the associated errors are often non-Gaussian and asymmetric, especially for extreme values of t. This presents a problem in ascertaining the t dependence of the form factors in the two step process which must be used in the "unparametrized" methods of extracting either f_+ and ξ or f_+ and f_0 [fits (1) and (2)], since the *a posteriori* fit to the linear form factors hypothesis assumes that the errors on values at each t are Gaussian, and correlations between the form factors are not taken into account. The 2-parameter fit does not suffer from this problem since the two parameters are almost completely uncorrelated. This is illustrated by the error ellipses for λ_+ and λ_0 as shown in Fig. 18.

Several recent experiments have used unparametrized fits to extract the t dependence of the form factors. We believe that unparametrized fits should be used to indicate the appropriate functional forms to be applied in a parametrized fit. Thus we believe that our fits (1) and (2) should be taken to illustrate the validity of the assumption of linear t dependence for f_+ and f_0, and the constancy of ξ, but the 2-parameter fit (3) provides the most reliable method of extracting the values of λ_+ and λ_0 from the Dalitz-plot data.

As can be seen from Fig. 15, the data show a tendency for ξ to take on increasingly positive values as $t \to 0$ in the unparametrized fit. This effect is correlated with the fact that the extrapolated value of $f_0(t)/f_+(0)$ at $t=0$ does not equal unity. It is worth pointing out that this behavior occurs in a region of t where the determination of ξ is relatively poor and the sensitivity to systematic errors quite high. Thus we do not believe that the data warrant a conclusion that the behavior of the form factors departs from a linear variation at low values of t. The satisfactory χ^2 for 2-parameter fit supports the statement that the data are adequately described by linearly varying f_+ and f_0 form factors.

VIII. COMPARISON WITH MONTE CARLO AND STUDY OF SYSTEMATIC ERRORS

It is clear that the Dalitz-plot analysis depends crucially on our being able to reproduce faithfully the experimental conditions in the Monte Carlo programs. A great deal of effort went into ensuring that the Monte Carlo events were as realistic as possible. In this section we compare some of the observed "primary" distributions for the accepted events with the Monte Carlo predictions. One should note that the effect of any discrepancies observed in these distributions on the actual Dalitz-plot population should be considerably diluted by the Lorentz transformation from the laboratory to the K_L^0 center-of-mass system.

To test quantitatively the effect of any possible experimental bias on our final result, we have introduced various possible biases into the data and then refitted the resulting Dalitz plot using the linear parametrization of the form factors. Typically, we have tried to introduce a distortion about four times higher than warranted by the data. The results of these tests are listed in Table VII and are discussed below in connection with specific distributions. We note that some of the distortions

TABLE VI. Dependence of the results of the 2-parameter (λ_+, λ_0) fit on the form factors used in the Monte Carlo calculation.

Change in Monte Carlo form factor			Effect on 2-parameter-fit result		
$\Delta\lambda_+$	$\Delta\lambda_0$	$[\Delta\xi(0)]$	$\Delta\chi^2$	$\Delta\lambda_+$	$\Delta\lambda_0$
0.02	0.00	0.00	16.6	0.0014	0.0016
0.00	−0.04	−0.5	3.4	0.0037	−0.0074

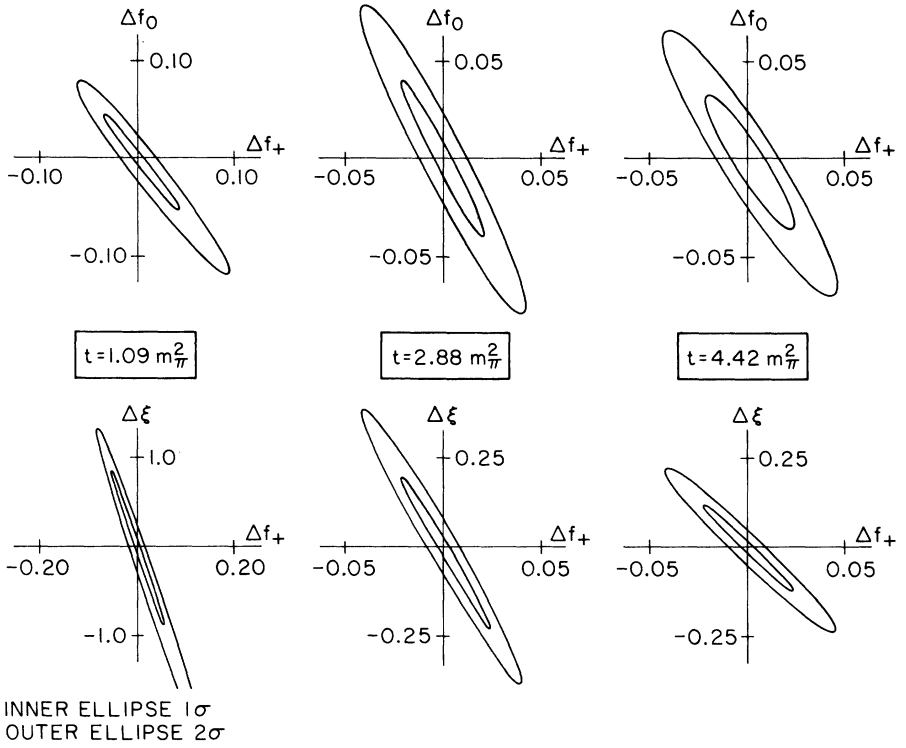

FIG. 17. Error ellipses of f_0 vs f_+ and ξ vs f_+ for three different values of t.

introduced do not significantly alter the χ^2 for the over-all fit but do have appreciable effects on the values of the fitted parameters. Therefore, it is important to assure ourselves that these systematic effects are indeed absent, by a detailed comparison of the many experimental distributions with the Monte Carlo predictions.

One can point to several specific inputs that must be correctly reproduced by the Monte Carlo program if one hopes to calculate the correct efficiencies. These inputs are

(1) momentum spectrum of K_L^0's,
(2) precision of time-of-flight information,
(3) precision of geometrical reconstruction,
(4) wire-chamber efficiency as a function of position and angle,
(5) counter efficiencies, and
(6) Coulomb scattering of muons in the lead.

We shall present comparisons between the Monte Carlo and experimental distributions and discuss the significance of each comparison in relation to these points. To provide a quantitative estimate of the quality of agreement between the data and the Monte Carlo distribution, we will quote a χ^2 and number of degrees of freedom for each distribution. A number of the points in some of the distributions contain in excess of 10^5 events; their statistical error is thus a few parts times 10^{-3} of the number of events in that bin. We do not feel that we are free of biases at that level, nor do we need to be, even for an experiment with our precision. Thus in computing the errors for the purpose of calculating a χ^2, we have placed a lower limit of 2% of the number of events on the quoted error. Therefore,

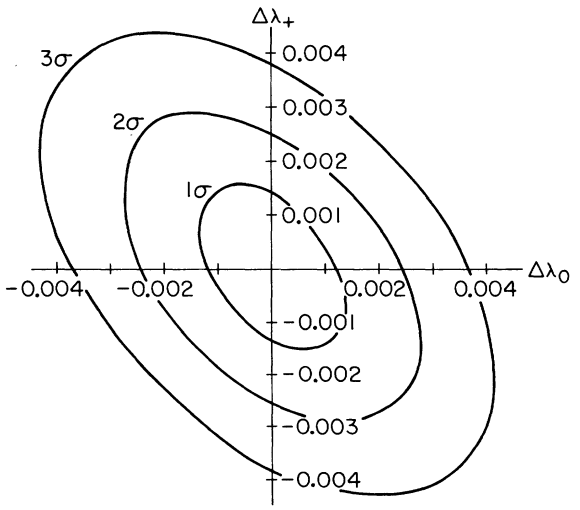

FIG. 18. Error ellipses for the 2-parameter fit.

TABLE VII. Investigation of the effect of possible systematic biases. The alterations described were in each case a factor of 4 larger than could be reasonably accommodated by the data.

Alteration of data	$\Delta\chi^2$	$\Delta\lambda_+$	$\Delta\lambda_0$	$\Delta\xi(t=5.2)$	$\Delta\xi(t=1.6)$
50% loss of events with $P_\pi < 1.25$ GeV/c	1.3	−0.0010	−0.0007	−0.041	−0.017
Excess of 10% of events with $P_K < 6$ GeV/c	−4.2	0.0026	0.0026	−0.010	−0.142
Excess of 10% of events with $6.5 < P_K < 8.5$ GeV/c	19.1	0.0001	−0.0002	0.005	0.008
Excess of 10% of events with $P_K > 10$ GeV/c	17.9	−0.0009	−0.0004	−0.004	0.073
Measured time of flight increased by 60 psec	−4.1	0.0042	0.0017	0.147	−0.289
Time-of-flight error increased by 40%	4.9	−0.0011	−0.0005	0.046	0.151
Additional ±2 mrad uncertainly folded into directional cosines of charged tracks	99.0	0.0036	−0.0057	0.057	−0.407
Beam direction altered by 1 mrad	49.0	0.0017	−0.0032	0.012	−0.144
50% loss of events with $T7$	−3.1	0.0000	−0.0001	0.004	0.007
50% excess of events with $C2$	52.8	0.0009	−0.0014	−0.023	0.087
50% loss of events with $C8$	154.7	0.0012	−0.0007	−0.058	0.234
Events with large μ Coulomb scatter eliminated	7.1	0.0001	−0.0021	−0.046	−0.055
$\pi \to \mu\nu$ decay correction increased by 20%	2.2	−0.0003	−0.0034	−0.010	−0.215
Air and veto counter diffraction scattering increased by a factor of 2	−5.1	−0.0010	−0.0004	0.001	−0.030
Point source of K^0 beam used in Monte Carlo	12.5	−0.0007	0.0004	0.163	0.272
No correction for pion penetration	1.1	−0.0002	0.0023	0.032	0.064

a reasonable χ^2 for a given number of degrees of freedom should be interpreted as an agreement between the data and the Monte Carlo calculations at the level of 2% or better.

A. K_L^0 momentum spectrum

The plots of the reconstructed K_L^0 momentum and the measured momenta of the pion and muon are shown in Fig. 19. As discussed in Sec. V A, the input K_L^0 momentum to the Monte Carlo calculations was adjusted to obtain agreement with the reconstructed momenta in Fig. 19(a). The pion and muon momenta were then also reproduced quite well by the Monte Carlo calculations. The excess χ^2 for the pion momentum distribution is due partly to a slight deficiency in the experiment of events with $P_\pi < 1.5$ GeV/c, corresponding to an inefficiency of about 4%, and partly to a deficiency of high energy pions.

We have tested the sensitivity of the results to a small change in the K_L^0 momentum spectrum by augmenting in turn three different parts of the spectrum by 10%. These results are illustrated in Table VII. Similarly, any possible inefficiency at low P_π was simulated by introducing a 50% inefficiency for $P_\pi < 1.25$ GeV/c.

B. Precision of the time-of-flight measurement

The comparison of the difference between the measured and fitted K_L^0 TOF is displayed in Fig. 20. As the Monte Carlo timing error was adjusted to reproduce the experimental distribution, the agreement should not be taken as an independent check, but rather as a demonstration of the accuracy with which the final Monte Carlo TOF error was chosen.

Figures 21 and 22 illustrate the missing mass squared and the reconstructed K_L^0 mass. These two distributions are particularly sensitive to the precision of the TOF measurement. The sensitivity of λ_+ and λ_0 to the TOF precision was tested by shifting the measured TOF systematically by 60 psec, and also by increasing the TOF uncertainty by 40%. The results are given in Table VII.

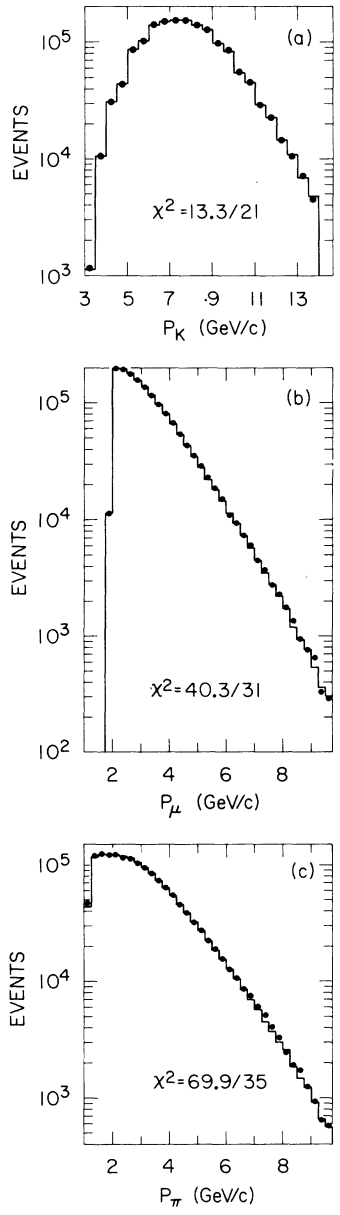

FIG. 19. Laboratory momentum spectra for (a) K_L^0, (b) μ, and (c) π.

C. Precision of geometrical reconstruction

Figure 23 shows the plots of $p_\nu^\perp - p_\nu^*$ for several different bands of p_ν^*. This quantity can take on positive values only because of experimental resolution or the presence of background. Thus the shape of the spectrum at low positive values of $p_\nu^\perp - p_\nu^*$ is a good measure of the experimental resolution. We would like to emphasize here that the experimental resolution in this context includes not only the measurement and Coulomb-scattering errors on the two charged tracks, but also the un-

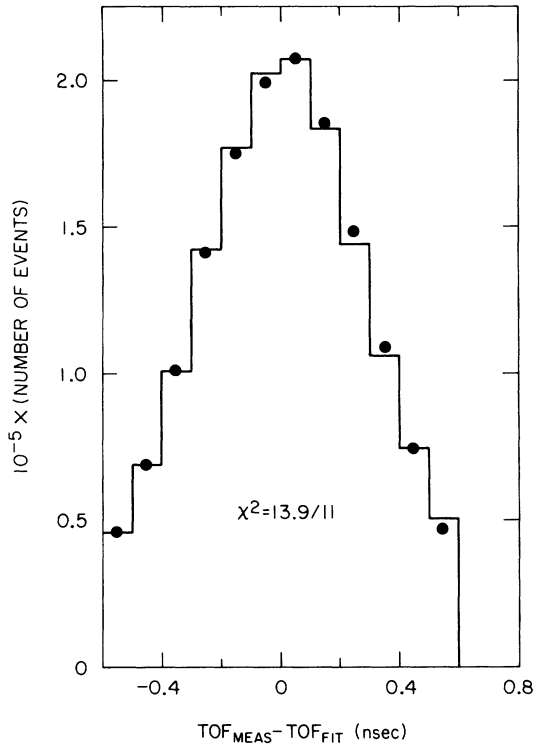

FIG. 20. Difference between the measured and fitted K_L^0 time-of-flight spectrum.

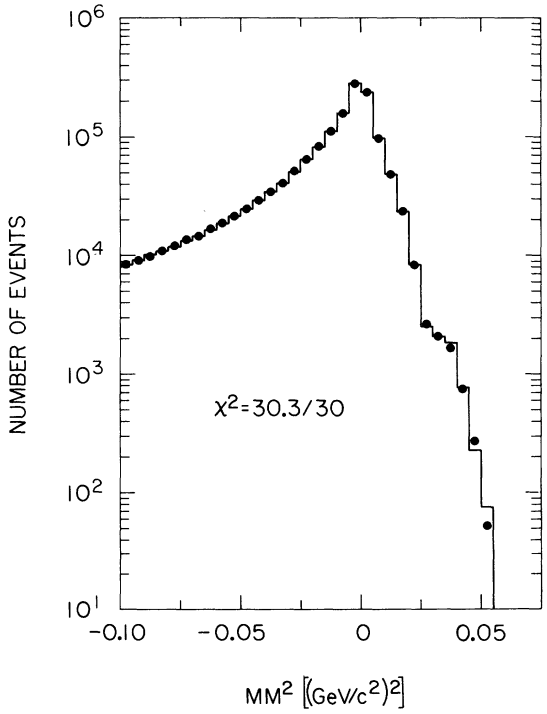

FIG. 21. Missing mass squared distribution.

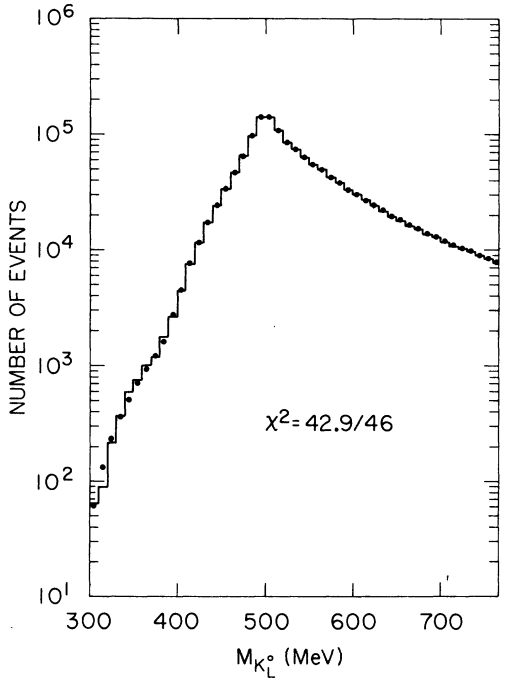

FIG. 22. Reconstructed K^0_L mass spectrum.

certainty in the K^0_L direction due to scattering in the Pb filter or the collimators. The good agreement in the falloff region illustrates our understanding of the experimental resolution.

The effective mass of the $\pi\mu$ spectrum is shown in Fig. 24. The agreement near the kinematic limit $m_{\pi\mu} = m_K$ is an independent verification of the faithful reproduction of the experimental errors in the Monte Carlo calculations. We note here that no sharp departures from smoothness are seen anywhere in the spectrum; more specifically, no excess of events is seen around $m_{\pi\mu} \approx 420$ MeV/c^2, in contrast with some previous observations.[23] The experimental resolution in this region is about ± 3 MeV/c^2.

In order to test the sensitivity of the results to the directional information, we have systematically altered the K^0_L direction by 1 mrad. In an independent test we have increased the error on the upstream X and Y direction cosines of the π and μ (α_π, β_π, α_μ, β_μ) by folding in a ± 2-mrad random spread to the measured values. The results are given in Table VII.

D. Efficiency of the wire chambers

A great deal of effort was expended in ensuring that the chambers were highly efficient over the entire fiducial area, regardless of the number of sparks. Rather than discuss some of these tests, we limit ourselves to illustrating the agreement of various observed track distributions with the Monte Carlo predictions. Figure 25 presents the

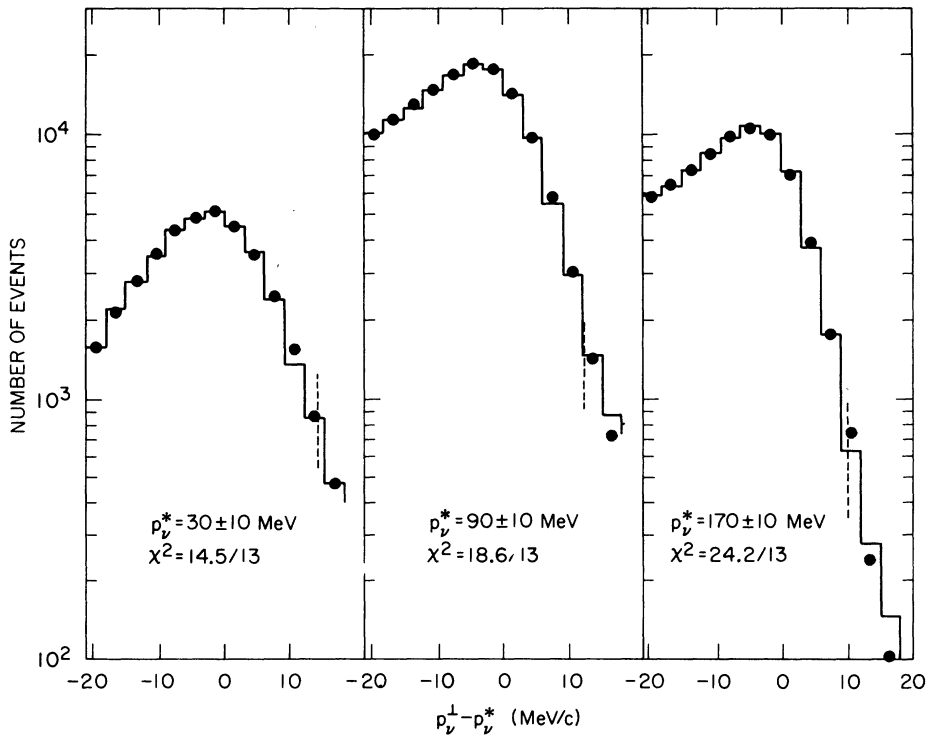

FIG. 23. Distribution of $p^\perp_\nu - p^*_\nu$ for three different bands of p^*_ν. The dashed lines indicate the cuts applied to the data.

direction cosines in the horizontal (α) and vertical (β) planes of the pion and the muon, both upstream and down stream of the magnet. We specifically call attention to the good agreement of α_π in the rear, which has the largest dynamic range. Software inefficiency or an imperfect understanding of the vertical focusing of the magnet would tend to cause depletion in the data at large values of α_π.

A comparison was made between the data and Monte Carlo in the two dimensional distributions which resulted from projecting each charged track onto the plane of each wire chamber. No significant deficiencies were found in any region. Figure 26 presents the X and Y projection distributions of the two charged tracks in the center of the upstream and downstream chambers. The excess χ^2 for the front chamber distributions is due entirely to a deficiency of about 7% at the outer edges which contain less than 1% of the events. The fact that this kind of inefficiency could not cause any significant bias was ascertained by refitting the data with greatly reduced acceptance as described in subsection G of this section.

E. Counter efficiency

Because of the poor duty cycle of SLAC, the resolving time of the coincidence and latch circuits used in the experiment had been set to ~±4 nsec. One might therefore expect some counter inefficiencies due to timing jitter. Clearly, these losses would in no way affect the experiment, provided that they were the same for all counters.

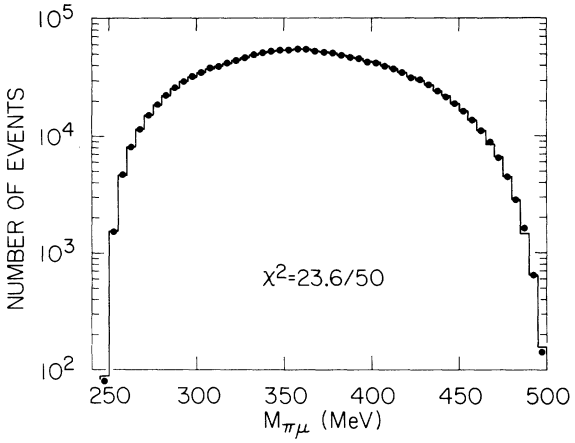

FIG. 24. $\pi\mu$ effective mass distribution.

The timing tests and adjustments were made in such a manner as to ensure that all the timing circuits were properly timed to ±1 nsec. The efficiency of the A counters could be extracted from the 2 TRACK data, since only a single A counter was required in the trigger. That efficiency, of the order of 97%, was found to be constant to $\pm\frac{1}{2}\%$ over all twelve A counters.

The ultimate test of the satisfactory performance of all the counters is again the agreement of their counting rates with the Monte Carlo prediction. The distributions of the T, A, B, and C counters are shown in Fig. 27. The T counter distribution has been folded twice through the horizontal and vertical axes of symmetry; the other three counter

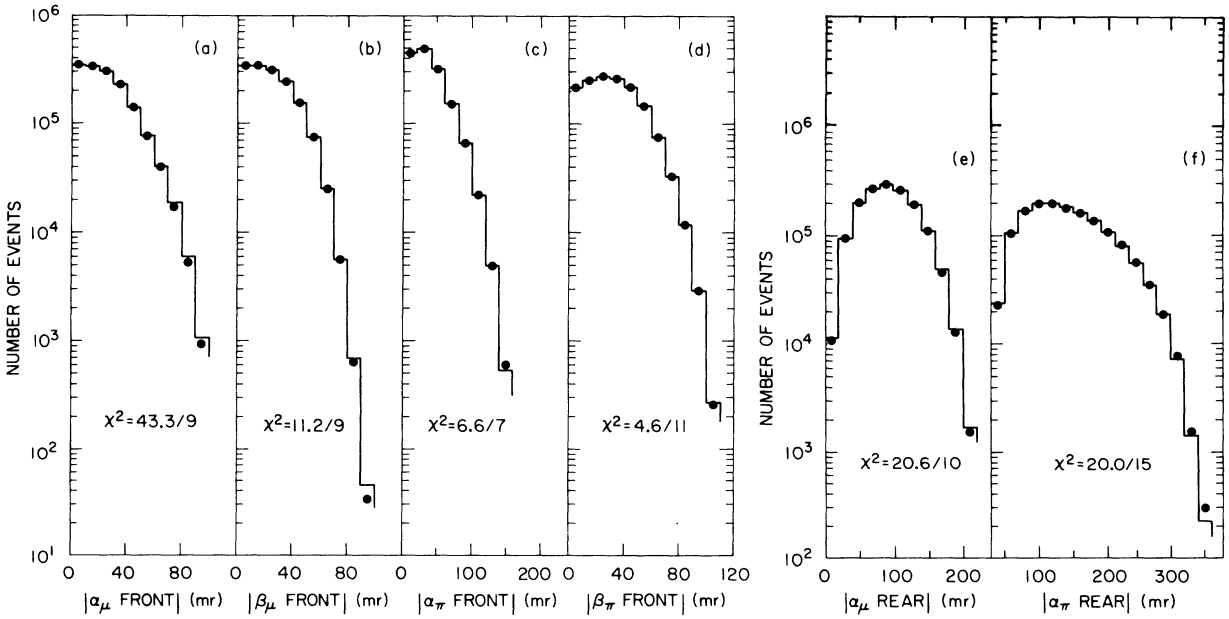

FIG. 25. Distribution of absolute values of X and Y direction cosines (a), (b) of the μ in front chambers; (c), (d) of the π in front chambers. (e), (f) Absolute values of X direction cosines of the μ and π in rear chambers.

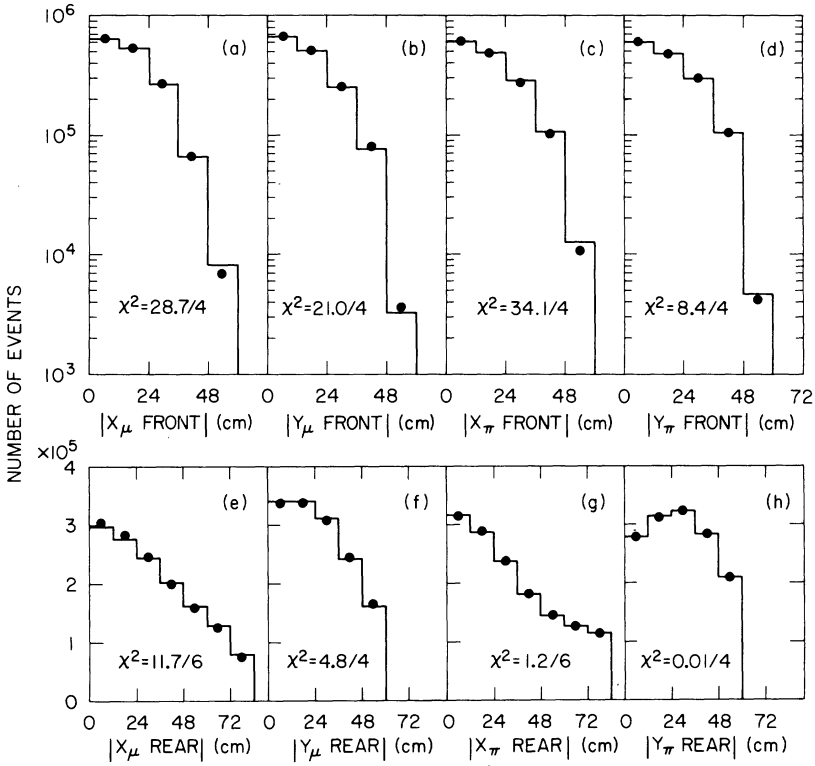

FIG. 26. Distribution of absolute values of X and Y coordinates (a), (b) of the μ in front chambers; (c), (d) of the π in front chambers; (e), (f) of the μ in rear chambers; and (g), (h) of the π in rear chambers.

banks have been folded about the vertical axis. The major sources of discrepancies are manufacturing tolerances in the scintillator widths (±0.32 mm in 15 cm), small gaps between the counters in a hodoscope bank, timing jitter in the coincidence and latch timing circuits due to electronic effects as well as to differences in flight paths, and dead-time effects due to high instantaneous rates.

To test the sensitivity of our results to counter inefficiency, we have successively introduced an inefficiency of 50% in C8, an excess of 50% in C2, and an inefficiency of 50% in T7. The effect of these variations is shown in Table VII.

F. Coulomb scattering of muons in the lead filter

It is important that the Coulomb scattering of the muons be faithfully reproduced in the Monte Carlo calculations, since it was possible to lose events through leakage of muons through the sides of the lead filter, or through a scattering larger than that allowed by the software. The quality of agreement of the Coulomb scattering is indicated by the plots in Fig. 28, which show the difference in the projected and observed muon X coordinates at the C counter bank for muons in three different momentum ranges. The observed muon position was taken to be the center of the struck C counter.

The width as a function of momentum is reproduced quite well, except for a relatively constant background, typically of the order 1% of the number of events in the peak. Possible sources of this effect are large single scatters, which were not included in the Monte Carlo calculations, accidentals, and pion penetration. Note that the last two effects have been corrected for in the Dalitz-plot analysis, but no effort was made to include these corrections in the distributions of Fig. 28. As a test of the sensitivity of our results to any anomalous tail, we have eliminated events with $\Delta X > 80$ cm$/P_\mu$ (GeV$/c$), and then subjected the remaining data to the 2-parameter fit. The results are shown in Table VII.

Finally, we present in Fig. 29 the Z distribution of the decay vertices of the accepted events. This distribution is sensitive to the K_L^0 momentum spectrum, as well as to the geometrical acceptance of the apparatus.

G. Estimate of systematic errors

The data presented in Table VII allow us to estimate the systematic errors due to the possible biases and uncertainties, as discussed above. Since the biases could have either sign, we can

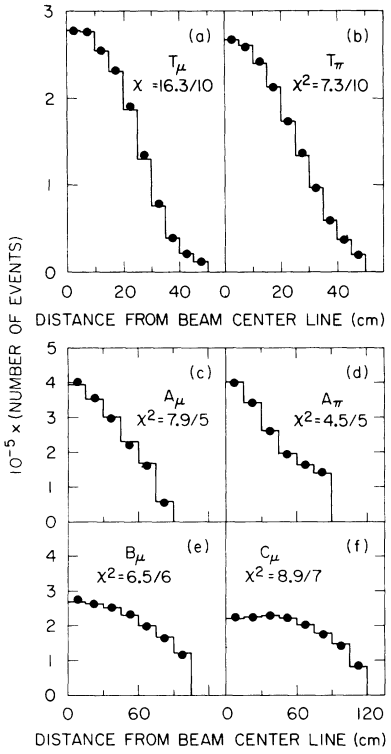

FIG. 27. Distribution (a), (b) of μ and π counts in T counters; (c), (d) of μ and π counts in A counters; and (e), (f) of μ counts in B and C counters.

add all the changes in λ_+ and λ_0 in quadrature. Dividing by the enhancement factor of 4 (because the systematic distortions introduced in Table VII are about a factor of 4 higher than warranted by the data), we obtain as the estimate of our systematic errors

$$\delta\lambda_+^{\text{syst}} = 0.0016\,, \qquad \delta\lambda_0^{\text{syst}} = 0.0022\,. \tag{34}$$

This procedure probably overestimates the errors, since it is quite likely that some of the effects illustrated by Figs. 19–29 are correlated.

We also show in Table VII the sensitivity of ξ in two different bins of t to various systematic changes in the data. The well-known fact that the sensitivity of the data to ξ is poor at low t is quite apparent. In general, we also find that the values of λ_+ and λ_0 obtained from the unparametrized fits tend to vary considerably more than the values of these parameters obtained from the 2-parameter fit.

To search for other possible systematic effects we have performed several further tests. The first of these consisted of performing the 2-parameter fit on several different subsets of data. In particular, the following different subsets have been generated:

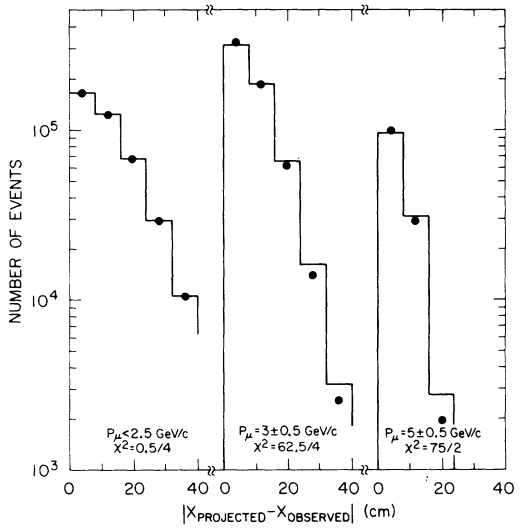

FIG. 28. Difference between the projected and observed X distribution of the μ in the C counters for three different bands of μ momentum.

(1) The data were divided into three subsets, depending on the difference between the two kinematic solutions. The first subset consisted of events in which both solutions yielded values of T_π and T_μ in the same 5×5 MeV bin. The second subset included only those events in which the *a priori* probability of one solution, as obtained from the TOF information and the $P(P_K, Z)$ matrix, was at least 20 times higher than the other. The remaining events formed the third subset.

(2) The events were divided according to the fitted K_L^0 momentum, the three subsets corre-

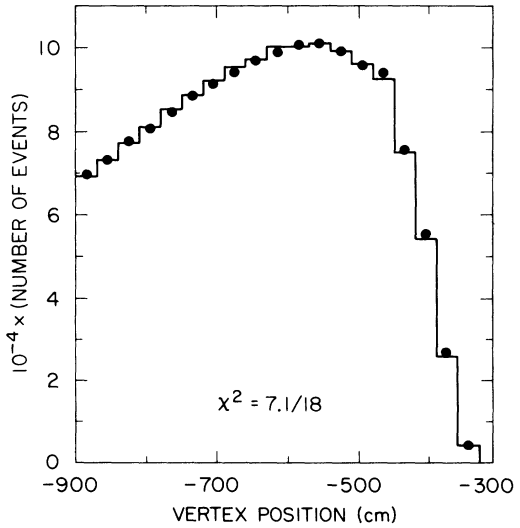

FIG. 29. Z distribution of the decay vertex.

sponding to $P_K < 6.5$ GeV/c, 6.5 GeV/$c < P_K < 8.5$ GeV/c, and $P_K > 8.5$ GeV/c.

(3) The inbending (U) and outbending (V) events were treated separately. The U events tend to give muons in the central C counters, the V events in the outer ones.

(4) Events with muons striking one side of the C bank ($C \leq 8$) were treated separately from events striking the other ($C > 8$).

(5) Events with positive and negative muons were fitted separately.

(6) The two subsets of data were fitted independently.

In the interest of computer-time economy, only the first subset of data was used in generating subsets (1)–(3).

The results of these fits are given in Table VIII. It can be seen that the values of λ_0 are quite consistent with what we might expect from statistical fluctuations alone: $\chi^2 = 8.1$ for 8 degrees of freedom. On the other hand, there is a larger spread of λ_+ values ($\chi^2 = 32.0$ for 8 degrees of freedom). We should stress, however, that no systematic effects have been included in Table VIII; any such systematics would tend to affect these individual subsets much more strongly than they would the total data. Hence we do not feel that these fluctuations are evidence of any systematic biases beyond those specifically discussed.

As an example, we might point to the subset of data that consists of events in which both solutions fall in the same 5 × 5 MeV bin. These events have a very transverse neutrino and thus a good possibility of failing to satisfy $p_\nu^* > p_\nu^\perp$. We would expect this subset to be quite sensitive to measurement errors. This is indeed the case; the variation of λ_+ as a function of measurement errors for this subset is almost a factor of 4 larger than for all the data.

The second set of tests consisted of modifying the selection criteria for the accepted events. We have made the following changes:

(1) The choice between the two kinematic solutions was made solely on the basis of which solution gave a TOF that was closer to the measured TOF.

(2) The choice between the two kinematic solutions was made solely on the basis of the more likely solution as determined from the $P(P_K, Z)$ matrix.

(3) The accepted events were required to pass through the center part of the magnet. Approximately 30% of the events near the edges were eliminated.

(4) The fitting procedure was repeated using the data grouped in 10 × 10 MeV bins.

TABLE VIII. Results of 2-parameter (λ_+, λ_0) fit to different subsets of data. Errors shown are statistical only.

Subset	χ^2	NDF [a]	λ_+	λ_0
Both solutions in the same bin	417	373	0.0177 ± 0.0038	0.0175 ± 0.0035
Ratio of 2 probs > 20	266	274	0.0422 ± 0.0052	0.0225 ± 0.0045
Remaining events	430	398	0.0304 ± 0.0020	0.0146 ± 0.0021
Low P_K	379	379	0.0390 ± 0.0030	0.0187 ± 0.0032
Medium P_K	406	398	0.0319 ± 0.0026	0.0146 ± 0.0025
High P_K	432	392	0.0233 ± 0.0030	0.0178 ± 0.0028
V events	380	398	0.0271 ± 0.0028	0.0182 ± 0.0026
U events	429	398	0.0315 ± 0.0020	0.0180 ± 0.0020
$C \leq 8$	437	398	0.0305 ± 0.0019	0.0170 ± 0.0019
$C > 8$	458	398	0.0306 ± 0.0020	0.0177 ± 0.0020
μ^+	379	398	0.0305 ± 0.0019	0.0180 ± 0.0019
μ^-	457	398	0.0305 ± 0.0019	0.0168 ± 0.0019
First subset of data	459	398	0.0303 ± 0.0015	0.0204 ± 0.0016
Second subset of data	412	398	0.0302 ± 0.0015	0.0179 ± 0.0016

[a] NDF ≡ number of degrees of freedom.

TABLE IX. Results of 2-parameter (λ_+, λ_0) fit using different selection criteria.

Modification	$\Delta\lambda_+$	$\Delta\lambda_0$
TOF information used only	−0.0030	−0.0008
P_K, Z information used only	0.0004	0.0002
Central part of the magnet used only	−0.0001	0.0000
10 by 10 MeV bins	0.0005	−0.0018

The results are displayed in Table IX. No significant departures from the original values are seen either in λ_+ or λ_0.

Finally, we have checked the stability of the results to cuts on T_μ, the muon kinetic energy in the K_L^0 center-of-mass system. The results of the 2-parameter fits under these conditions are shown in Table X.

IX. COMPARISON WITH PREVIOUS RESULTS

The results of the present experiment are in agreement with predictions of SU(2)⊗SU(2) and SU(3)⊗SU(3) symmetry for the scalar form factor f_0, and with the hypothesis that the vector form factor f_+ satisfies an unsubtracted dispersion relation which is saturated by the $K^*(890)$ pole. In this section, we review previous experimental determinations of these form factors for comparison with these ideas and other basic assumptions of $V-A$ Cabibbo theory. We have not attempted a global fit to all data with bearing on the t dependence of the form factors, but rather we have investigated Dalitz-plot density, branching ratio, and μ polarization measurements separately, including the latest results known to us. This is, therefore, essentially an updating of the compilation of Gaillard and Chounet,[24] in that we have found world averages for the linearly parametrized fits of the various experiments; we have not attempted to extract the form factors in an unparametrized way by combining data of different experiments as in the later review of CGG.[4] In cases where the χ^2 of the fit for N results is greater than 1 per degree of freedom, we have multiplied the quoted uncertainty by $\chi^2/(N-1)$, in an attempt to include the effects of presumed systematic errors. In cases where an experimental result differs by more than two standard deviations from the world average, we also quote results with that experiment discarded.

A. K_{e3} Dalitz-plot measurements

The K_{e3} Dalitz-plot distribution provides information on the validity of the assumption of a pure vector interaction, and allows extraction of the t dependence of the vector form factor. Under restrictive assumptions (e.g., that the induced scalar term f_S and the tensor term f_T are independent of t, and that they do not interfere) limits of $|f_S/f_+|<0.13$ (90% confidence level)[25] and $|f_T/f_+|<0.22$ (68% confidence level)[26] have been found. The present experiment places a very stringent limit on f_T: $|f_T/f_+(0)|<0.016$ at the 95% confidence level (see Sec. VII). We have compiled 11 K_{e3}^+ Dalitz-plot experiments and 14 K_{e3}^0 Dalitz-plot experiments which assume a vector interaction and extract λ_+, either from the two dimensional distribution or from the pion or electron energy spectrum alone. These results, together with the best least-squares fit, are shown in Table XI (Refs. 25, 27–50) and Fig. 30. The K_{e3}^+ experiments yield a good χ^2 and a mean value $\lambda_+ = 0.029 \pm 0.005$, while the K_{e3}^0 experiments yield a poor χ^2 and a mean value $\lambda_+ = 0.032 \pm 0.004$. With the Firestone *et al.*[39] and Albrow *et al.*[48] results discarded, the K_{e3}^0 result is $\lambda_+ = 0.030 \pm 0.004$, with a somewhat improved χ^2 of 18.1 for 10 degrees of freedom. Results for both K_{e3}^+ and K_{e3}^0 are thus seen to be in excellent agreement with the K^* dominance prediction. The agreement between the K_{e3}^+ and K_{e3}^0

TABLE X. Results of 2-parameter (λ_+, λ_0) fit to different areas of the Dalitz plot. Errors shown are statistical only.

Subset	χ^2	NDF	λ_+	λ_0
$T_\mu < 65$ MeV	126	153	0.0236 ± 0.0030	0.0219 ± 0.0034
$T_\mu > 65$ MeV	252	240	0.0333 ± 0.0019	0.0188 ± 0.0016
2 edge bins eliminated from each q^2 bin	283	307	0.0340 ± 0.0020	0.0141 ± 0.0026

TABLE XI. Determination of λ_+ from K^+_{e3} and K^0_{e3} Dalitz plot, or from pion or lepton energy spectra.

		K^+_{e3}				K^0_{e3}	
Experiments	Ref.	λ_+	Number of events	Experiment	Ref.	λ_+	Number of events
Brown *et al.* (1962)	27	0.036 ± 0.045	175	Luers *et al.* (1964)	37	0.07 ± 0.06	153
Jensen *et al.* (1964)	28	-0.010 ± 0.029	407	Fischer *et al.* (1965)	38	0.15 ± 0.08	577
Borreani *et al.* (1964)	29	-0.040 ± 0.050	230	Firestone *et al.* (1967)	39	-0.01 ± 0.02	764
Belloti *et al.* (1967)	30	$0.045^{+0.017}_{-0.018}$	854	Kadyk *et al.* (1967)	40	0.01 ± 0.015	531
Kalmus *et al.* (1967)	31	0.028 ± 0.014	515	Lowys *et al* (1967)	41	$0.08^{+0.10}_{-0.08}$	240
Imlay *et al.* (1967)	32	0.016 ± 0.016	1393	Kulyukina *et al.* (1967)	42	$0.03^{+0.055}_{-0.040}$	394
Botterill *et al.* (1968)	33	0.080 ± 0.040	17 000	Aronson *et al.* (1968)	43	0.020 ± 0.013	824–1020
Eisler *et al.* (1968)	34	$-0.020^{+0.080}_{-0.120}$	90	Basile *et al.* (1968)	44	0.023 ± 0.012	4800
Botterill *et al.* (1970)	35	0.045 ± 0.015	1458	Bisi *et al.* (1971)	45	0.023 ± 0.005	42 000
Steiner *et al.* (1971)	36	0.027 ± 0.010	2707	Dally *et al.* (1972)	46	0.05 ± 0.01	10 000
Chiang *et al.* (1972)	25	0.029 ± 0.011	4017	Neuhofer *et al.* (1972)	47	0.022 ± 0.014	1910
Average		0.029 ± 0.005		Albrow *et al.* (1972)	48	0.055 ± 0.010	6668
				Buchanan *et al.* (1972)	49	0.044 ± 0.006	26 000
$\chi^2 = 8.2$ for 10 degrees of freedom				Brandenburg *et al.* (1973)	50	0.019 ± 0.013	1871
				Average		0.032 ± 0.004	
				$\chi^2 = 28.1$ for 13 degrees of freedom			

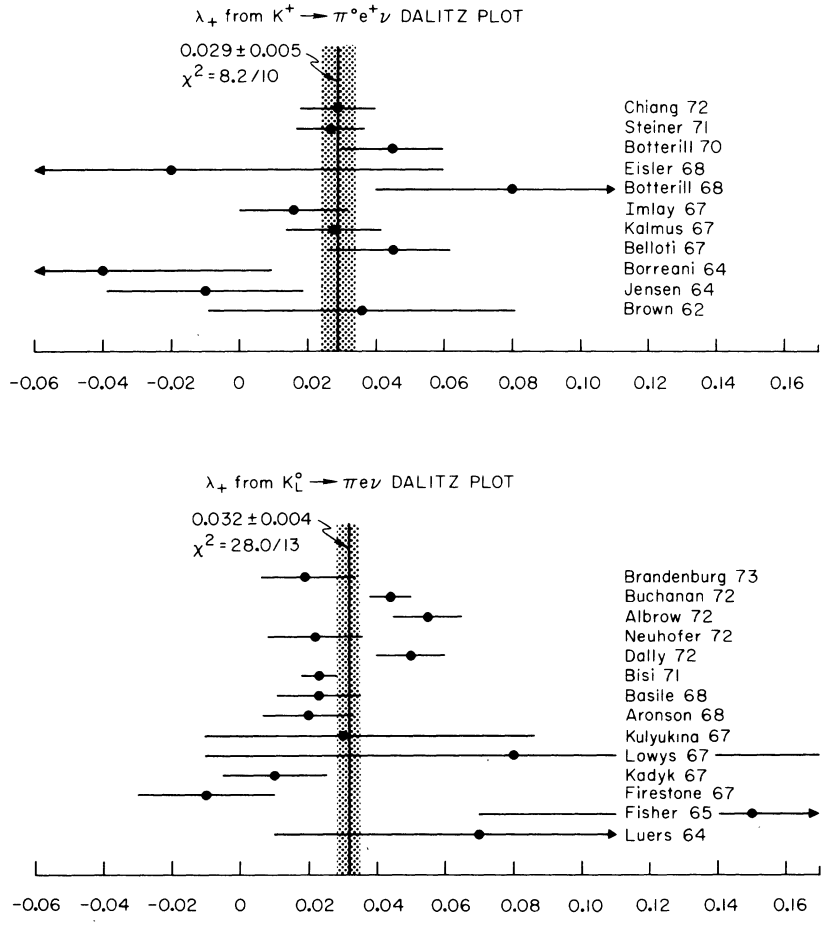

FIG. 30. Determination of λ_+ in K^+_{e3} and K^0_{e3} Dalitz plot from pion or electron energy-spectra analyses.

values for λ_+ is also experimental confirmation of the $|\Delta I| = \frac{1}{2}$ rule. It should be noted, however, that radiative corrections have been applied to very few of these experiments, and in those cases where they have, the effect of apparatus efficiency has not been correctly incorporated. The limited statistics of even the best of these experiments, however, makes it unlikely that inclusion of the radiative corrections would significantly alter the results.

B. $K_{\mu 3}$ Dalitz-plot measurements

The $K_{\mu 3}$ Dalitz-plot distribution, as we have seen, provides information on the two form factors of the matrix element. Until recently, most experiments have been analyzed in terms of f_+ and ξ. In comparing the various experiments, we have followed this convention. Many experiments have presented their results in several forms, with varying assumptions or constraints. To facilitate the comparison of results, we have, wherever possible, chosen to compare analyses in terms of λ_+ and $\xi(0)$, with $\lambda_- \equiv 0$. To the level of precision of the experiments treated here, the results are quite insensitive to the value of λ_-, and further, $\lambda_- = 0$ corresponds to the assumption of linear t dependence of f_0. In a few instances, it has been necessary to employ the correlation functions presented by the authors in order to calculate a result for $\lambda_- = 0$. Chiang *et al.*[25] present no such correlation, so their result has been included in the form $\xi(0)$, $\lambda_+ \equiv \lambda_-$. In Fig. 31 and Table XII

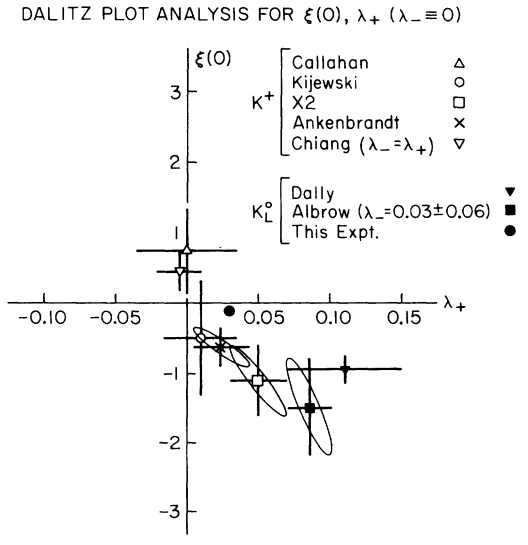

FIG. 31. Results of λ_+, $\xi(0)$ fits (with $\lambda_- \equiv 0$) to $K^+_{\mu 3}$ and $K^0_{\mu 3}$ Dalitz plots. Error ellipses are shown for three experiments.

TABLE XII. Values of $\xi(0)$, λ_+ from $K^+_{\mu 3}$ or $K^0_{\mu 3}$ Dalitz-plot analyses (with $\lambda_- \equiv 0$). Several experiments did not perform 2-parameter fits, but found $\xi(0)$ with λ_+ fixed to a particular value (usually 0).

	$K^+_{\mu 3}$				$K^0_{\mu 3}$			
Experiment	Ref.	Number of events	$\xi(0)$	λ_+	Experiment	Ref.	Number of events	$\xi(0)$	λ_+
Brown *et al.* (1962)	27	76	1.46 ± 1.2	$\equiv 0$	Carpenter *et al.* (1966)	54	1371	1.2 ± 0.8	$\equiv 0$
Jensen *et al.* (1964)	28	≈120	-0.50 ± 0.7	$\equiv 0$	Basile *et al.* (1970)	55	3140	-3.9 ± 0.1	$\equiv 0$
Callahan *et al.* (1966)	51	444	0.72 ± 0.50	0.00 ± 0.035	Chien *et al.* (1970)	56	26 500	$-0.68^{+0.12}_{-0.20}$	0.090 ± 0.02
Eisler *et al.* (1968)	34	78	-0.50 ± 0.9	$\equiv 0$	Dally *et al.* (1972)[b]	46	16 500	-0.94 ± 0.18	0.11 ± 0.04
Kijewski (1969)	52	2041	-0.5 ± 0.8	0.009 ± 0.026	Albrow *et al.* (1973)[c]	57	9066	-1.5 ± 0.7	0.085 ± 0.015
X2 collaboration (1971)	26	3240	-1.1 ± 0.5	0.050 ± 0.019	Peach *et al.* (1973)	58	1385	-0.90 ± 0.45	$\equiv 0.025$
Ankenbrandt *et al.* (1972)	53	4025	-0.62 ± 0.28	0.024 ± 0.022	This experiment (1974)		1.6×10^6	-0.11 ± 0.04	0.030 ± 0.003
Chiang *et al.* (1972)[a]	25	3900	0.45 ± 0.28	-0.006 ± 0.015					

[a] $\lambda_- \equiv \lambda_+$. [b] Note that the data of Ref. 46 are a subset of those of Ref. 56. [c] $\lambda_- = 0.030 \pm 0.060$.

(Refs. 25–28, 34, 46, 51–58) we present these results for $K^+_{\mu 3}$ and $K^0_{\mu 3}$. We have plotted only results of true 2-parameter fits. It is clear that the results are so inconsistent as to render any world average meaningless. In any case, such a world average would be totally dominated by the present experiment, which has more than 60 times the statistics of any previous $K_{\mu 3}$ Dalitz-plot analysis. Also, to our knowledge, none of the previous analyses has included radiative corrections, although again it is unlikely that this has had any significant effect on the results.

C. Branching-ratio measurements

The ratio of the rates $\Gamma(K \to \pi\mu\nu)/\Gamma(K \to \pi e\nu)$ determines a relation between the two form factors. Thus, if f_+ and f_0 are assumed to have linear t dependence, $\Gamma_{\mu 3}/\Gamma_{e3}$ determines a point in the (λ_+, λ_0) plane. For completeness, we display below this relation for K^+ and K^0_L decays:

$$\frac{\Gamma^+_{\mu 3}}{\Gamma^+_{e3}} = \frac{0.646 + 2.228\lambda_+ + 4.321\lambda_+^2 + 1.573\lambda_0 + 3.405\lambda_0^2 - 0.914\lambda_+\lambda_0}{1 + 3.700\lambda_+ + 5.478\lambda_+^2},$$
$$\frac{\Gamma^0_{\mu 3}}{\Gamma^0_{e3}} = \frac{0.645 + 2.081\lambda_+ + 3.885\lambda_+^2 + 1.465\lambda_0 + 3.074\lambda_0^2 - 1.027\lambda_+\lambda_0}{1 + 3.457\lambda_+ + 4.779\lambda_+^2}. \quad (35)$$

In finding a world average for $\Gamma^+_{\mu 3}/\Gamma^+_{e3}$, we have followed the procedure of Gaillard and Chounet (GC) in adjusting published values of $\Gamma^+_{\mu 3}/\Gamma^+_{e3}$ for the effect of cuts necessary to exclude background. We have therefore corrected $\Gamma^+_{\mu 3}$ and Γ^+_{e3} rates independently, and then used average values of these separate rates to determine $\Gamma^+_{\mu 3}/\Gamma^+_{e3}$. GC found the fraction of the $K^+_{\mu 3}$ Dalitz plot observed in the experiments using the values $\lambda_+ = 0.03$ and $\xi(0) = -1$. In the light of our experimental findings, we have recalculated this correction factor using $\lambda_+ = 0.03$ and $\xi(0) = 0.0$. Our correction factors are compared with the GC factors for $\Gamma^+_{\mu 3}$ in Table XIII.[25,26,51,59–70] No significant changes were introduced by this procedure. We find $\Gamma^+_{\mu 3} = (3.08 \pm 0.08)\%$ with a poor χ^2 of 20.6 for 12 degrees of freedom (see Fig. 32). Exclusion of the Cutts *et al.*[66] and *X*2[26] experiments changes this result to $\Gamma^+_{\mu 3} = (3.18 \pm 0.07)\%$ with a greatly improved χ^2 of 7.9 for 10 degrees of freedom.

The GC analysis used a value of $\lambda_+ = 0.03$ to extrapolate the measured Γ^+_{e3} partial rates to total rates. We concur in this choice, and therefore our compilation differs from theirs only in the

TABLE XIII. Determination of $K^+_{\mu 3}$ branching ratio ($\Gamma^+_{\mu 3}$). Corrections to be made for cuts necessary to exclude background are compared for $\lambda_+ = 0.03$, $\xi = -1$ (GC values) and for $\lambda_+ = 0.03$, $\xi = 0$.

Experiment	Ref.	Number of events	Partial rate correction GC($\xi = -1$)	$\xi = 0$	$\Gamma^+_{\mu 3}$ (%)
Birge *et al.* (1956)	59	7			
Alexander *et al.* (1957)	60	12	0.708	0.711	3.7 ± 0.9
Bøggild *et al.* (1961)	61	6			
Taylor *et al.* (1959)	62	37	0.280	0.287	2.8 ± 0.5
Giacomelli *et al.* (1964)	63	87	0.154	0.159	3.6 ± 0.5
Shaklee *et al.* (1964)	64	≈120	Not corrected		3.0 ± 0.5
Bisi *et al.* (1965)	65	2100 + 745	Error increased to account for background		3.52 ± 0.40
Cutts *et al.* (1965)	66	489	0.064	0.064	4.12 ± 0.6
Callahan *et al.* (1966)	51	636	Not corrected		2.83 ± 0.19
Auerbach *et al.* (1967)	67	310	0.454	0.448	3.10 ± 0.28
Botterill *et al.* (1968)	68	5600	Not corrected		3.23 ± 0.10
Garland *et al.* (1968)	69	350	0.757	0.750	3.02 ± 0.24
Zeller *et al.* (1969)	70	≈30	Not corrected		3.44 ± 0.6
*X*2 collaboration (1971)	26	1505	0.292	0.290	2.78 ± 0.11
Chiang *et al.* (1972)	25	3900	Not corrected		3.33 ± 0.16
			Average		3.08 ± 0.08

$\chi^2 = 20.6$ for 12 degrees of freedom

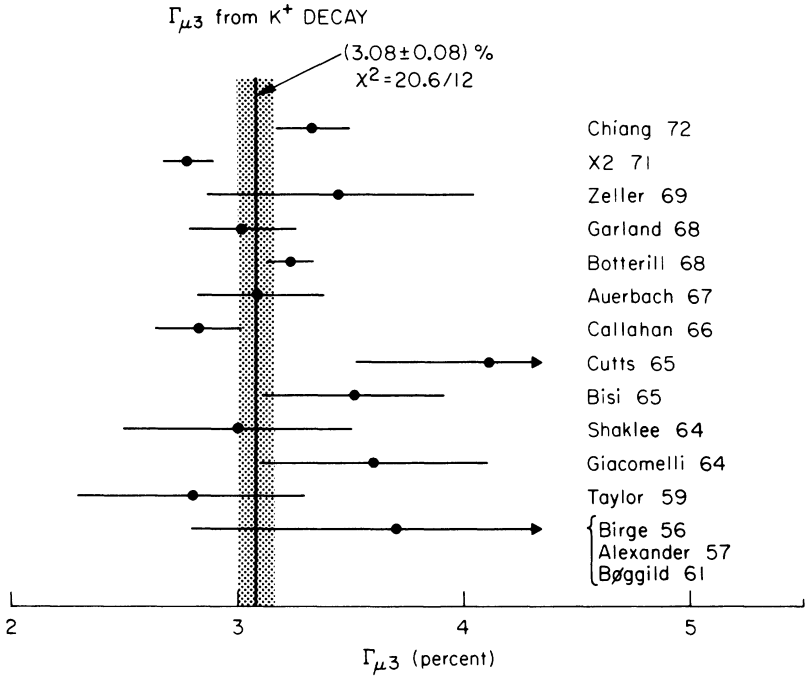

FIG. 32. Determination of the $K^+_{\mu 3}$ branching ratio.

inclusion of the new result of Chiang *et al.*[25] The summary of Γ^+_{e3} measurements is shown in Table XIV (Refs. 25, 26, 29, 30, 51, 59–61, 64, 67–73) and Fig. 33. We find $\Gamma^+_{e3} = (4.80 \pm 0.07)\%$, with a poor χ^2 of 25.9 for 15 degrees of freedom. If we exclude the experiment of Callahan *et al.*,[51] which differs from the mean by four standard deviations, we find $\Gamma^+_{e3} = (4.85 \pm 0.06)\%$, with a good χ^2 of 11.2 for 14 degrees of freedom.

For all experiments, therefore, we find $\Gamma^+_{\mu 3}/\Gamma^+_{e3} = 0.642 \pm 0.015$. If we fix $\lambda_+ = 0.03$, as indicated by K_{e3} Dalitz-plot analyses, this result implies $\lambda_0 = 0.000 \pm 0.011$, or $\xi(0) = -0.37 \pm 0.13$. Retaining only those experiments within 2σ of the world averages, we find $\Gamma^+_{\mu 3}/\Gamma^+_{e3} = 0.656 \pm 0.014$, which with $\lambda_+ \equiv 0.03$ yields $\lambda_0 = 0.011 \pm 0.010$ or $\xi(0) = -0.25 \pm 0.12$.

For the K^0_L branching ratios, which do not suffer from the same background problems as the K^+ decays, we have calculated $\Gamma^0_{\mu 3}/\Gamma^0_{e3}$ directly from the published ratios. These results are summarized in Table XV (Refs. 37, 50, 55, 74–82) and Fig. 34. Our result differs from GC only in that it includes the latest results of Evans *et al.*[82] and the new measurement of Brandenburg *et al.*[50] The world average is $\Gamma^0_{\mu 3}/\Gamma^0_{e3} = 0.695 \pm 0.017$ with a χ^2 of 9.3 for 11 degrees of freedom. With $\lambda_+ \equiv 0.03$, this gives $\lambda_0 = 0.035 \pm 0.010$ or $\xi(0) = +0.09 \pm 0.13$.

These world averages do not support the $\Delta I = \frac{1}{2}$ rule prediction $\Gamma^+_{\mu 3}/\Gamma^+_{e3} = \Gamma^0_{\mu 3}/\Gamma^0_{e3}$, but in view of the poor agreement of several of the experiments included in the world average, and the agreement of λ_+ as derived from K^+_{e3} and K^0_{e3} Dalitz-plot analyses, this discrepancy need not be viewed as being serious. The K^+ results favor $\lambda_0 \geq 0$, while the K^0_L results clearly require $\lambda_0 > 0$, in accord with the soft-pion prediction.

TABLE XIV. Determination of K^+_{e3} branching ratio (Γ^+_{e3}).

Experiment	Ref.	Γ^+_{e3} (%)
Birge *et al.* (1956)	59	3.2 ±1.3
Alexander *et al.* (1957)	60	5.1 ±1.3
Bøggild *et al.* (1961)	61	3.4 ±1.7
Roe *et al.* (1961)	71	5.0 ±0.5
Shaklee *et al.* (1964)	64	4.7 ±0.3
Borreani *et al.* (1964)	29	5.00±0.34
Callahan *et al.* (1966)	51	4.02±0.21
Young *et al.* (1967)	72	5.30±0.90
Belloti *et al.* (1967)	30	5.24±0.50
Auerbach *et al.* (1967)	67	4.93±0.16
Eschstruth *et al.* (1968)	73	5.17±0.19
Garland *et al.* (1968)	69	4.35±0.40
Botterill *et al.* (1968)	68	4.92±0.21
Zeller *et al.* (1969)	70	4.31±0.40
*X*2 collaboration (1971)	26	4.75±0.11
Chiang *et al.* (1972)	25	4.86±0.10
Average		4.80±0.07

$\chi^2 = 25.9$ for 15 degrees of freedom.

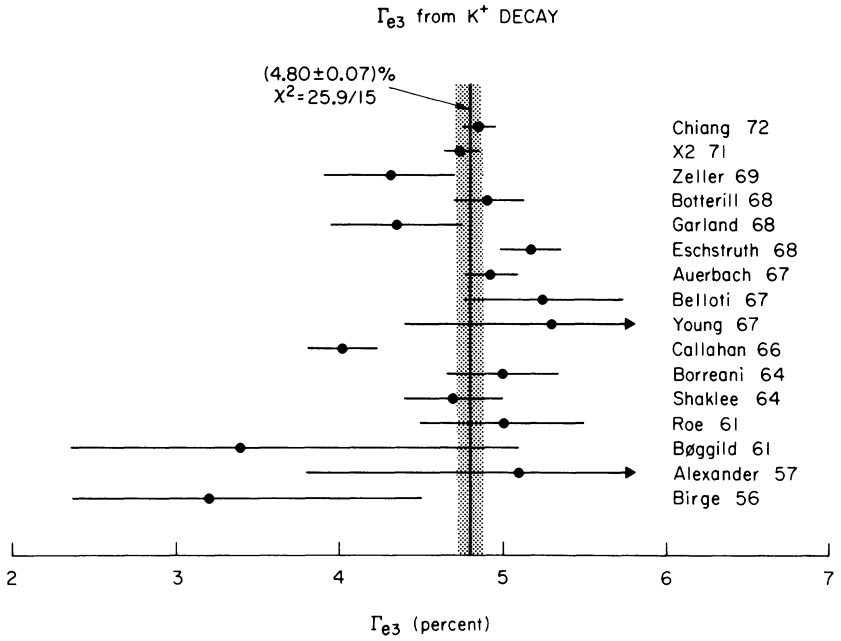

FIG. 33. Determination of the K^+_{e3} branching ratio.

D. $K_{\mu 3}$ polarization measurements

The only new muon polarization measurement since the CGG compilation is the result of Sandweiss *et al.*,[83] which is $\xi(0) = -0.385 \pm 0.105 - 6.0\lambda_+$, or $\xi(0) = -0.57 \pm 0.11$ with $\lambda_+ = 0.03$. Figure 35 and Table XVI (Refs. 26, 51, 52, 83–87) present K^+ and K^0_L muon polarization measurements, which give $\xi(0) = -0.94 \pm 0.21$ for K^+ with a χ^2 of 1.15 for 4 degrees of freedom, and $\xi(0) = -0.69 \pm 0.19$ for K^0_L with a poor χ^2 of 10.6 for 3 degrees of freedom. These values of $\xi(0)$ do not agree with that found by the branching-ratio method, with the trend of $\xi(0)$ as found in the $K_{\mu 3}$ Dalitz-plot analyses (Fig. 31), or with the present experiment. Further, the polarization results also do not agree very well with the various "rigorous" bounds,[13] especially those which include the soft-pion result as a constraint.

It is interesting to note that a possible resolution of the discrepancy between the Dalitz plot and branching ratio results for $\xi(0)$ on the one hand, and the muon polarization measurements on the other, may lie in the possibility of the existence of small scalar or tensor amplitudes in the matrix element. The direction of muon polarization in certain areas of the Dalitz plot is particularly sensitive to small admixtures of scalar amplitude,[88] which have not been excluded by present K_{e3} Dalitz-plot analyses below a level of about 15%. It appears that resolution of the situation will have to await high-statistics K_{e3} Dalitz-plot analyses and future muon-polarization experiments.

X. CONCLUSIONS

We have presented a detailed discussion of a high-statistics measurement of the Dalitz plot in $K^0_L \to \pi\mu\nu$ decay. Several parametrizations of the t dependence of the vector form factor f_+ and the scalar form factor f_0 have been studied. A thorough examination of possible systematic biases

TABLE XV. Determination of the ratio of $K^0_{\mu 3}$ to K^0_{e3} branching ratios ($\Gamma^0_{\mu 3}/\Gamma^0_{e3}$).

Experiment	Ref.	$\Gamma^0_{\mu 3}/\Gamma^0_{e3}$
Adair *et al.* (1964)	74	0.81 ±0.19
Luers *et al.* (1964)	37	0.73 ±0.15
Astbury *et al.* (1965)	75	0.85 ±0.25
de Bouard *et al.* (1967)	76	0.82 ±0.10
Hawkins *et al.* (1967)	77	0.70 ±0.20
Hopkins *et al.* (1967)	78	0.81 ±0.08
Kulyukina *et al.* (1968)	79	0.63 ±0.16
Budagov *et al.* (1968)	80	0.71 ±0.05
Beilliere *et al.* (1969)	81	0.70 ±0.04
Basile *et al.* (1970)	55	0.62 ±0.05
Evans *et al.* (1973)	82	0.662 ± 0.030
Brandenburg *et al.* (1973)	50	0.741 ± 0.044
Average		0.695 ± 0.017

$\chi^2 = 9.3$ for 11 degrees of freedom.

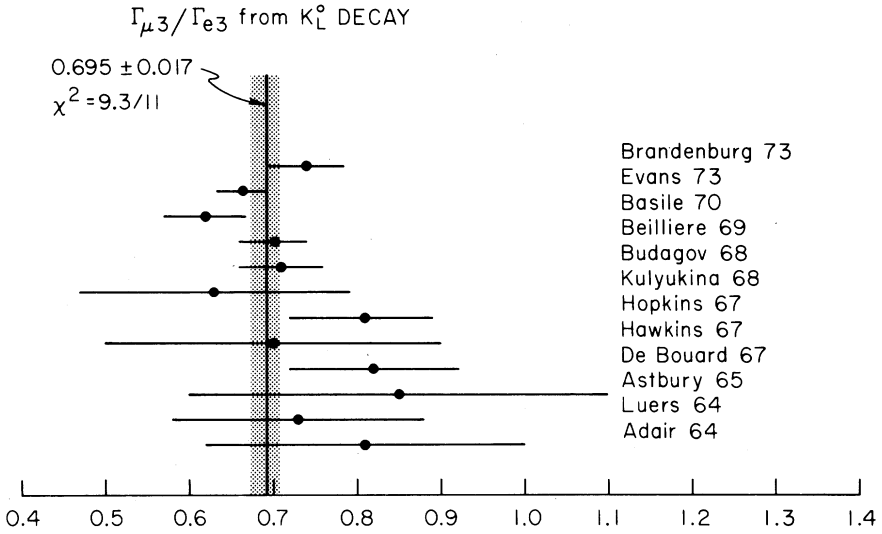

FIG. 34. Determination of $\Gamma^0_{\mu 3}/\Gamma^0_{e3}$.

has been made, allowing an estimate of their contribution to the uncertainties in the slopes of the form factors. Our analysis shows that both the vector and scalar form factors are well described by a linear t dependence in the physical region, with slopes

$$\lambda_+ = 0.030 \pm 0.003, \qquad \lambda_0 = 0.019 \pm 0.004, \tag{36}$$

where the uncertainties quoted are the sum of statistical and systematic errors. This value of λ_+ is consistent with $K^*(890)$ dominance of the

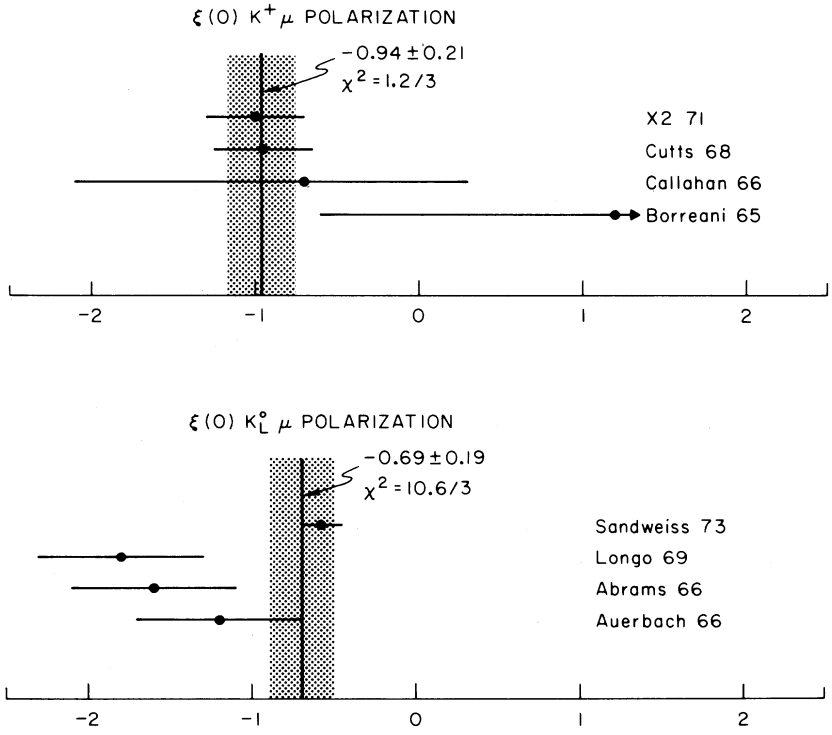

FIG. 35. Determination of $\xi(0)$ in $K^+_{\mu 3}$ and $K^0_{\mu 3}$ muon-polarization analyses.

TABLE XVI. Determination of $\xi(0)$ in $K^+_{\mu 3}$ and $K^0_{\mu 3}$ muon polarization analyses.

K^+				K^0_L			
Experiment	Ref.	$\xi(0)$	Number of events	Experiment	Ref.	$\xi(0)$	Number of events
Borreani *et al.* (1965)	84	$1.2^{+2.4}_{-1.8}$	2100	Auerbach *et al.* (1966)	85	-1.2 ± 0.5	2600
Callahan *et al.* (1966)	51	-0.7 ± 0.9	3347	Abrams *et al.* (1968)	86	-1.6 ± 0.5	665
Cutts *et al.* (1968)	52	-0.95 ± 0.30	3133	Longo *et al.* (1969)	87	-1.81 ± 0.50	
$X2$ collaboration (1971)	26	-1.00 ± 0.30	6000	Sandweiss *et al.* (1973)[a]	83	-0.57 ± 0.11	2.2×10^6
Average		-0.94 ± 0.21		Average		-0.69 ± 0.19	
$\chi^2 = 1.2$ for 3 degrees of freedom.				$\chi^2 = 10.6$ for 3 degrees of freedom.			

[a] $\lambda_+ = 0.03$.

vector form factor, and with current world averages for λ_+ as determined in studies of the K_{e3} Dalitz plot, in accord with μ-e universality. An extrapolation of f_0 using $\lambda_0 = 0.019$ yields a value of 1.22 ± 0.04 at $t = m_K{}^2 - m_\pi{}^2$, in excellent agreement with the Callan-Treiman-Mathur-Okubo-Pandit current algebra prediction (presented in its original derivation at $t = m_K{}^2$). The extrapolated slope of f_0 also confirms the prediction of Dashen and Weinstein. Our experimental results thus support the hypothesis that chiral SU(3)⊗SU(3) and SU(2)⊗SU(2) are good symmetries of the strong interactions, and that symmetry-breaking effects are small.

ACKNOWLEDGMENTS

We wish to thank M. Schwartz for his enthusiastic support of this effort, and to acknowledge the important contributions of R. Coombes and D. Porat to the construction and improvement of the spectrometer. We have also enjoyed helpful conversations with many of our colleagues, especially S. Brodsky, J. Smith, and M. Weinstein. Finally we acknowledge the excellent support of the Experimental Facilities, Accelerator Operations, and Computer Operations Group of the Stanford Linear Accelerator Center.

*Present address: Weizmann Institute of Science, Rehovoth, Israel.

†Work supported in part by the U. S. Atomic Energy Commission.

§Present address: Rockefeller University, New York, N. Y. 10021.

‖Alfred P. Sloan Foundation Fellow.

[1] R. Piccioni, G. Donaldson, D. Dorfan, D. Fryberger, D. Hitlin, J. Liu, R. Messner, B. Meyer, A. Rothenberg, M. Schwartz, D. Uggla, and S. Wojcicki, preceding paper, Phys. Rev. D 9, 2939 (1974).

[2] G. Donaldson, D. Fryberger, D. Hitlin, J. Liu, B. Meyer, R. Piccioni, A. Rothenberg, D. Uggla, S. Wojcicki, and D. Dorfan, Phys. Rev. Lett. 31, 337 (1973).

[3] R. Coombes, D. Fryberger, D. Hitlin, R. Piccioni, D. Porat, and D. Dorfan, Nucl. Instrum. Methods 98, 317 (1972).

[4] L.-M. Chounet, J.-M. Gaillard, and M. K. Gaillard, Phys. Rep. 4C, 199 (1972).

[5] Our notation in this paper is as follows: Four-vectors are denoted by p_K, p_π, etc. Three-momenta and total energies in the kaon center-of-mass system are denoted by p^*_π, E^*_π, etc. The kinetic energies of the pion and muon in the kaon center-of-mass system are denoted by T_π and T_μ. Three-momenta and total energies in the laboratory frame are denoted by P_π, E_π, etc.

[6] M. J. Matison, LBL Report No. 1537, 1973 (unpublished).

[7] C. G. Callan and S. B. Treiman, Phys. Rev. Lett. 16, 153 (1966); V. S. Mathur, S. Okubo, and L. K. Pandit, *ibid.* 16, 371 (1966). This relation was originally derived using conventional PCAC techniques for f_0 at $t = m_K{}^2$. By changing the argument to $t = m_K{}^2 - m_\pi{}^2$, one obtains a result which is explicitly correct to first order in SU(2)⊗SU(2) symmetry breaking. See R. Dashen and M. Weinstein, Phys. Rev. Lett. 22, 1337 (1969).

[8] R. Dashen and M. Weinstein, Phys. Rev. Lett. 22, 1337 (1969).

[9] Determination of f_K/f_π requires a determination of $f_+(0)$, which is derived from the branching ratio $\Gamma(K^+ \to \pi^0 e^+ \nu)/\Gamma(K^+ \to \text{all})$. The value of $f_+(0)\sin\theta_C$ obtained from this branching ratio, however, depends on the value of λ_+ used to describe the variation of $f_+(t)$ on the K^+_{e3} Dalitz plot. We have used $\lambda_+ = 0.03$.

[10] R. Dashen, L.-F. Li, H. Pagels, and M. Weinstein, Phys. Rev. D 6, 834 (1972); B. G. Kenny and M. Kac, Phys. Rev. D 9, 826 (1974); B. Renner and U. Wam-

bach, Nucl. Phys. B54, 1 (1973).
[11]M. K. Gaillard, Nuovo Cimento 61, 499 (1969); R. A. Brandt and G. Preparata, Ann. Phys. (N.Y.) 61, 119 (1970), and references therein, *ibid.* Phys. Rev. D 7, 218 (1973).
[12]M. Weinstein, Phys. Rev. D 3, 481 (1971); G. Ecker, Nuovo Cimento 13A, 291 (1973). See, however, J. L. Newmeyer and S. D. Drell, Phys. Rev. D 8, 4070 (1973).
[13]S. Okubo and I-F. Shih, Phys. Rev. D 4, 2020 (1971); I-F. Shih and S. Okubo, *ibid.* 6, 1393 (1972); S. Okubo, *ibid.* 7, 1519 (1973); S. Okubo and Y. Ueda, *ibid.* 8, 1372 (1973); L.-F. Li and H. Pagels, *ibid.* 3, 219 (1971) C. Bourreley, Nucl. Phys. B43, 434 (1972); G. Ecker, Nuovo Cimento 13A, 291 (1973); B. Renner and U. Wambach, Nucl. Phys. B54, 1 (1973); U. M. Wambach, *ibid.* B53, 597 (1973); A. H. Kazi, II. Institut fur Theoretische Physik report, 1973 (unpublished); L. Tataru, Research Institute for Theoretical Physics report, 1973 (unpublished); K. Kang, P. X. Yem, and P. Pond, Nuovo Cimento Lett. 8, 825 (1973); J. S. Kang, Phys. Rev. D 7, 2636 (1973).
[14]The analysis programs have been discussed in detail in Paper I. Briefly, they consist of the following:
PASS 1: Forms tracks from sparks, calibrates ADC units, sets a single reference time for all TOF measurements.
PASS 2: Matches front and rear tracks, determines particle charge and momenta, finds muons, locates decay vertex, computes K_L^0 TOF.
PASS 3: Transforms 2 TRACK events to the K_L^0 center-of-mass system, places each event on the $K_{\mu 3}^0$ Dalitz plot, applies final cuts, updates histograms.
[15]The variable P_0^2, which is computed assuming the decay is a $K_{\pi 3}^0$ decay, is positive for $K_{\pi 3}^0$ and negative for K_{l3}^0 decays, in the absence of measurement errors. This variable was first used by A. Astier, L. Blaskovic, M. M. DeCourreges, B. Equer, A. Lloret, P. Rivet, and J. Siaud, in *Proceedings of the Aix-en-Provence Conference on Elementary Particles, 1961* (Centre d'Études Nucléaires de Saclay, Gif-sur-Yvette, Seine et Oise, Saclay, France, 1961), p. 227. (This work is available in English as SLAC Translation No. 143.)
[16]At the present time, there is some uncertainty in the value of the $K_{\pi 2}^0$ branching ratio. The value given by the Particle Data Group [Rev. Mod. Phys. 45, S1 (1973)] is 1.57×10^{-3}. However, a recent measurement with the SLAC K^0 spectrometer by R. Messner, R. Morse, U. Nauenberg, D. Hitlin, J. Liu, R. Piccioni, M. Schwartz, S. Wojcicki, and D. Dorfan [Phys. Rev. Lett. 36, 876 (1973)] gives 2.07×10^{-3}.
[17]R. Messner, A. Franklin, R. Morse, U. Nauenberg, D. Dorfan, D. Hitlin, J. Liu, and R. Piccioni, paper submitted to the XVI International Conference on High Energy Physics, Chicago-Batavia, Ill. (unpublished).
[18]The ionization energy loss, $-(dE/dx)$, for muons as a function of the muon energy was taken from W. P. Trower, LBL Report No. UCRL-2426, 1966 (unpublished).
[19]Particle Data Group, Rev. Mod. Phys. 45, S1 (1973).
[20]E. S. Ginsberg, Phys. Rev. D 1, 229 (1970).
[21]E. S. Ginsberg, Phys. Rev. 142, 1035 (1966); 162, 1570 (1967); 171, 1675 (1968); T. Becherrawy, Phys. Rev. D 1, 1452 (1970); A. N. Kamal and N. N. Wong, Nucl. Phys. B31, 48 (1971).
[22]H. W. Fearing, E. Fischbach, and J. Smith, Phys. Rev. D 2, 542 (1970).
[23]C. A. Ramm, Nature 227, 1323 (1970).
[24]M. K. Gaillard and L.-M. Chounet, CERN Report No. CERN 70-14, 1970 (unpublished).
[25]I-H. Chiang, J. L. Rosen, S. Shapiro, R. Handler, S. Olsen, and L. Pondrom, Phys. Rev. D 6, 1254 (1972).
[26]D. Haidt, J. Stein, S. Natali, G. Piscitelli, F. Romano, E. Fett, J. Lemonne, T. I. Pedersen, S. N. Tovey, V. Brisson, P. Petian, C. D. Esveld, J. J. M. Timmermans, B. Aubert, L.-M. Chounet, L. Dong, F. Babisut, H. Huzita, F. Sconza, A. Marzari-Chiesa, and A. E. Werbrouck ($X2$ Experiment), Phys. Rev. D 3, 10 (1971).
[27]J. L. Brown, J. A. Kadyk, G. H. Trilling, R. T. Van de Walle, B. P. Roe, and D. Sinclair, Phys. Rev. Lett. 8, 450 (1962).
[28]G. L. Jensen, F. S. Shaklee, B. P. Roe, and D. Sinclair, Phys. Rev. 136, B1431 (1964).
[29]G. Borreani, G. Rinaudo, and A. E. Werbrouck, Phys. Lett. 12, 123 (1964).
[30]E. Belloti, E. Fiorini, and A. Pullia, Nuovo Cimento 52A, 1287 (1967).
[31]G. E. Kalmus and A. Kernan, Phys. Rev. 159, 1187 (1967).
[32]R. L. Imlay, P. T. Eschstruth, A. D. Franklin, E. B. Hughes, D. H. Reading, D. R. Bowen, A. K. Mann, and W. K. McFarlane, Phys. Rev. 160, 1203 (1967).
[33]D. R. Botterill, R. M. Brown, A. B. Clegg, I. F. Corbett, G. Culligan, J. McL. Emmerson, R. C. Field, J. Garvey, P. B. Jones, N. Middlemas, D. Newton, T. W. Quirk, G. L. Salmon, P. Steinberg, and W. S. C. Williams, Phys. Rev. 174, 1661 (1968).
[34]F. R. Eisler, S. Y. Fung, S. L. Marateck, S. L. Meyer, and R. J. Plano, Phys. Rev. 169, 1090 (1968).
[35]D. R. Botterill, R. M. Brown, A. B. Clegg, I. F. Corbett, G. Culligan, J. McL. Emmerson, R. C. Field, J. Garvey, P. B. Jones, N. Middlemas, D. Newton, T. W. Quirk, G. L. Salmon, P. H. Steinberg, and W. S. C. Williams, Phys. Lett. 31B, 325 (1970).
[36]H. J. Steiner, S. Natali, F. Romano, D. C. Cundy, J. Lemonne, T. I. Pedersen, P. Rinton, L. Behr, V. Brisson, L. Kluberg, P. Petian, A. Aubert, J. P. Lowys, J. J. M. Timmermans, H. Huzita, F. Mattioli, A. Sconza, D. Gamba, and A. Marzari-Chiesa, Phys. Lett. 36B, 521 (1971).
[37]D. Luers, I. S. Mittra, W. J. Willis, and S. S. Yamamoto, Phys. Rev. 133, B1276 (1964).
[38]G. P. Fisher, A. Abashian, R. J. Abrams, D. W. Carpenter, B. M. K. Nefkens, J. H. Smith, and A. Wattenberg, in Proceedings of the International Conference on Weak Interactions, Argonne, 1965 (unpublished).
[39]A. Firestone, J. K. Kim, J. Lach, J. Sandweiss, H. D. Taft, and P. Guidoni, Phys. Rev. Lett. 18, 176 (1967).
[40]J. A. Kadyk, J. H. Chan, D. Drijard, Y. Oren, and B. M. Sheldon, Phys. Rev. Lett. 19, 597 (1967).
[41]J. P. Lowys, B. Aubert, L.-M. Chounet, C. Pascaud, and L. Behr, Phys. Lett. 24B, 75 (1967).
[42]L. A. Kulyukina, A. N. Mestvirishvili, D. Neagu, N. I. Petrov, V. A. Rusakov, and W. Chung-fan, Zh. Eksp. Teor. Fiz. 52, 90 (1967) [Sov. Phys.—JETP 25, 58 (1967)].
[43]S. H. Aronson and K. W. Chen, Phys. Rev. 175, 1708 (1968).

[44]P. Basile, J. W. Cronin, B. Thevenet, R. Turlay, S. Zylberajch, and A. Zylberszteijn, Phys. Lett. 26B, 542 (1968).
[45]V. Bisi, P. Darriulat, M. I. Ferrero, C. Grosso-Pilcher, K. Kleinknecht, C. Rubbia, A. Staude, and K. Tittel, Phys. Lett. 36B, 533 (1971).
[46]E. Dally, P. Innocenti, E. Seppi, C.-Y. Chien, B. Cox, L. Ettlinger, L. Resvanis, R. A. Zdanis, C. D. Buchanan, D. J. Drickey, F. D. Rudnick, P. F. Shepard, D. H. Stork, and H. K. Ticho, Phys. Lett. 41B, 647 (1972).
[47]G. Neuhofer, F. Niebergall, M. Regler, H. E. Stier, K. Winter, J. J. Aubert, X. DeBouard, V. Lepeltier, L. Massonnet, H. Pessard, M. Vivargent, T. R. Willitts, M. Yvert, W. Bartl, and M. Steuer, Phys. Lett. 41B, 642 (1972).
[48]M. G. Albrow, D. Aston, D. P. Barber, L. Bird, R. J. Ellison, C. H. Halliwell, R. E. H. Jones, A. D. Kanaris, F. K. Loebinger, P. G. Murphy, M. G. Strong, J. Walters, and D. D. Yovanovich, Nucl. Phys. B58, 22 (1973).
[49]C. D. Buchanan, D. J. Drickey, F. D. Rudnick, P. F. Shepard, D. H. Stork, H. K. Ticho, E. Dally, P. Innocenti, E. Seppi, C.-Y. Chien, B. Cox, L. Ettlinger, L. Resvanis, and R. A. Zdanis, Brookhaven Conference, 1972 (unpublished).
[50]G. W. Brandenburg, W. B. Johnson, D. W. G. S. Leith, J. S. Loos, J. A. J. Matthews, F. C. Winkelmann, and R. J. Yamartino, Phys. Rev. D 8, 1978 (1973).
[51]A. C. Callahan, U. Camerini, R. D. Hantman, R. H. March, D. L. Murphree, G. Gidal, G. E. Kalmus, W. M. Powell, C. L. Sandler, R. T. Pu, S. Natali, and M. Villani, Phys. Rev. 150, 1153 (1966).
[52]P. Kijewski, LBL Report No. 18433, 1969 (unpublished).
[53]C. Ankenbrandt, R. Larsen, L. Leipuner, L. Smith, F. Shively, R. Stefanski, R. Adair, H. Kasha, S. Merlan, R. Turner, and P. Wanderer, Phys. Rev. Lett. 28, 1472 (1972).
[54]D. W. Carpenter, A. Abashian, R. J. Abrams, G. P. Fisher, B. M. K. Nefkens, and J. H. Smith, Phys. Rev. 142, 871 (1966).
[55]P. Basile, J. W. Cronin, B. Thevenet, R. Turlay, S. Zylberajch, and A. Zylberszteijn, Phys. Rev. D 2, 78 (1970).
[56]C.-Y. Chien, B. Cox, L. Ettlinger, L. Resvanis, R. A. Zdanis, E. Dally, P. Innocenti, E. Seppi, C. D. Buchanan, D. J. Drickey, F. D. Rudnick, P. F. Shepard, D. H. Stork, and H. K. Ticho, Phys. Lett. 33B, 627 (1970).
[57]M. G. Albrow, D. Aston, D. P. Barber, L. Bird, R. J. Ellison, C. H. Halliwell, R. E. H. Jones, A. D. Kanaris, F. K. Loebinger, P. G. Murphy, M. G. Strong, J. Walters, and D. D. Yovanovich, Nucl. Phys. B44, 1 (1972).
[58]K. J. Peach, G. R. Evans, J. Muir, H. W. K. Hopkins, and W. Krenz, Phys. Lett. 43B, 441 (1973).
[59]R. W. Birge, D. H. Perkins, J. R. Peterson, D. H. Stork, and M. N. Whitehead, Nuovo Cimento 4, 834 (1956).
[60]G. Alexander, R. H. W. Johnston, and C. O'Ceallaigh, Nuovo Cimento 6, 478 (1957).
[61]J. K. Bøggild, K. H. Hansen, J. E. Hooper, M. Scharff, and P. K. Aditya, Nuovo Cimento 19, 621 (1961).
[62]S. Taylor, G. Harris, J. Orear, J. Lee, and P. Baumel, Phys. Rev. 114, 359 (1959).
[63]G. Giacomelli, D. Monti, G. Quareni, A. Quareni-Vignudelli, W. Püschel, and J. Tietge, Nuovo Cimento 34, 1134 (1964).
[64]F. S. Shaklee, G. L. Jensen, B. P. Roe, and D. Sinclair, Phys. Rev. 136, B1423 (1964).
[65]V. Bisi, G. Borreani, A. Marzari-Chiesa, G. Rinaudo, M. Vigone, and A. E. Werbrouck, Phys. Rev. 139, B1068 (1965).
[66]D. Cutts, T. Elioff, and R. Stiening, Phys. Rev. 138, B969 (1965).
[67]L. B. Auerbach, J. MacG. Dobbs, A. K. Mann, W. K. McFarlane, D. H. White, R. Cester, P. T. Eschstruth, G. K. O'Neill, and D. Yount, Phys. Rev. 155, 1505 (1967).
[68]D. R. Botterill, R. M. Brown, A. B. Clegg, I. F. Corbett, G. Culligan, J. McL. Emmerson, R. C. Field, J. Garvey, P. B. Jones, N. Middlemas, D. Newton, T. W. Quirk, G. L. Salmon, P. H. Steinberg, and W. S. C. Williams, Phys. Rev. Lett. 21, 766 (1968).
[69]R. Garland, K. Tsipis, S. Devons, J. Rosen, D. Tycko, L. G. Pondrom, and S. L. Meyer, Phys. Rev. 167, 1225 (1968).
[70]M. E. Zeller, R. P. Haddock, J. A. Helland, J. Pahl, N. T. Dairiki, R. L. Beck, K. M. Crowe, and M. T. Maung, Phys. Rev. 182, 1420 (1969).
[71]B. P. Roe, D. Sinclair, J. L. Brown, D. A. Glaser, J. A. Kadyk, and G. H. Trilling, Phys. Rev. Lett. 7, 346 (1961).
[72]P.-S. Young, W. Z. Osborne, and W. H. Barkas, Phys. Rev. 156, 1464 (1967).
[73]P. T. Eschstruth, A. D. Franklin, E. B. Hughes, R. L. Imlay, D. H. Reading, D. R. Bowen, and A. K. Mann, Phys. Rev. 165, 1487 (1968).
[74]R. K. Adair and L. B. Leipuner, Phys. Lett. 12, 67 (1964).
[75]P. Astbury, G. Finocchiaro, R. D. Fortune, A. Michelini, C. Virkerk, C. H. West, W. Beusch, M. Pepin, and M. A. Pouchon, Phys. Lett. 16, 80 (1965).
[76]X. de Bouard, D. Dekkers, B. Jordan, R. Mermod, B. Scharff, L. Valentin, M. Vivargent, T. R. Willitts, K. Winter, and M. Bott-Bodenhausen, Nuovo Cimento 52A, 662 (1967).
[77]C. J. B. Hawkins, Phys. Rev. 156, 1444 (1967).
[78]H. W. K. Hopkins, T. C. Bacon, and F. R. Eisler, Phys. Rev. Lett. 19, 185 (1967).
[79]L. A. Kulyukina, A. N. Mestvirishvili, D. Neagu, N. I. Petrov, V. A. Rusakov, and W. Tsung-fan, Zh. Eksp. Teor. Fiz. 53, 29 (1967) [Sov. Phys.—JETP 26, 20 (1968)].
[80]I. A. Budagov, H. Burmeister, D. C. Cundy, W. Krenz, G. Myatt, F. A. Nezrick, H. Sletten, G. H. Trilling, W. Venus, H. Yoshiki, B. Aubert, P. Heusse, I. DeLong, E. Nagy, C. Pascaud, L. Behr, P. Beilliere, G. Boutang, and J. Vander Velde, Nuovo Cimento, 57A, 182 (1968).
[81]P. Beilliere, G. Boutang, and J. Limon, Phys. Lett. 30B, 202 (1969).
[82]G. R. Evans, J. Muir, and K. J. Peach, Phys. Rev. D 7, 36 (1973).
[83]J. Sandweiss, J. Sunderland, W. Turner, W. Willis, and L. Keller, Phys. Rev. Lett. 30, 1002 (1973).
[84]G. Borreani, G. Gidal, G. Rinaudo, A. E. Werbrouck, A. Caforio, C. M. Garelli, S. Natali, and M. Villani, Phys. Rev. 140, B1686 (1965).
[85]L. B. Auerbach, A. K. Mann, W. K. McFarlane, and

F. J. Sciulli, Phys. Rev. Lett. 17, 980 (1966).
[86]R. J. Abrams, A. Abashian, R. E. Mischke, B. M. K. Nefkens, J. H. Smith, R. C. Thatcher, L. J. Verhey, and A. Wattenberg, Phys. Rev. 176, 1603 (1968).
[87]M. J. Longo, K. K. Young, and J. A. Helland, Phys. Rev. 181, 1808 (1969).
[88]J. Smith (private communication).

PHYSICAL REVIEW D VOLUME 9, NUMBER 11 1 JUNE 1974

Study of the decay distributions of the η' meson*

C. Baltay, D. Cohen, S. Csorna, M. Habibi,† and M. Kalelkar
Columbia University, New York, New York 10027

W. D. Smith and N. Yeh
State University of New York at Binghamton, Binghamton, New York 13901

(Received 5 March 1974)

We have carried out a study of the decay distributions of $\eta'(958)$ mesons produced in the reaction $K^- p \to \Lambda \eta'$ at 1.75 GeV/c, utilizing both the $\eta\pi^+\pi^-$ and $\pi^+\pi^-\gamma$ decay modes of the η'. A Dalitz-plot analysis of the $\eta\pi^+\pi^-$ decay channel rules out all spin-parity assignments except 0^- and 2^-, but is unable to distinguish between them. We find no evidence for the existence of anisotropies in the η' decay angular distributions, and thus our data do not support the recent conjecture, based on the observation of such anisotropies, that the η' has spin 2.

I. INTRODUCTION

The $\eta'(958)$ meson was discovered about 10 years ago,[1] and many subsequent investigations have sought to determine its spin-parity assignment.[2] Dalitz-plot analyses of the η' decays have ruled out all assignments except $J^{PC} = 0^{-+}$ and 2^{-+}, with the 0^{-+} assignment being favored. Since a spin-zero particle must decay isotropically in its center of mass, various attempts have been made to find evidence for a spin different from zero by searching for anisotropies in the η' decay distributions. Until recently, all such attempts proved fruitless, thus lending strong support to the 0^- spin-parity assignment of the η'. A Brookhaven-Michigan collaboration,[3] however, has recently studied the decay angular distributions of η' mesons produced in the extreme forward direction in the reaction $K^- p \to \Lambda \eta'$ at 2.18 GeV/c. They have found evidence that these forward-produced η' mesons have anisotropic decay distributions with respect to the incident beam, suggesting the possibility that the η' has $J^P = 2^-$. The confirmation of this spin-parity assignment would, of course, force us to revise the current SU(3) particle-classification scheme, which has the η' belonging to the pseudoscalar-meson nonet along with the π, K, and η mesons.

We have carried out a study of the decay distributions of the η' meson utilizing the reaction $K^- p \to \Lambda \eta'$ at an incident K^- momentum of 1.75 GeV/c. We have performed an analysis of the η' Dalitz plot and find the distribution of events to be consistent with only the 0^{-+} and 2^{-+} J^{PC} assignments for the η'. We have also searched for anisotropies in the decay angular distributions of forward-produced η' mesons. Unlike the Brookhaven-Michigan analysis, we do not find any evidence for the existence of such anisotropies, and thus our data do not lend additional support to the hypothesis of a spin-2 η' suggested by their analysis.

II. EXPERIMENTAL PROCEDURE

The data used in the present analysis are derived from an exposure of the Brookhaven National Laboratory 31-in. hydrogen bubble chamber to a beam of 1.75-GeV/c K^- mesons. The particular sample discussed here represents approximately 60% of the total exposure of 860 000 pictures and corresponds to ~23 events/μb. All two-pronged events with an associated neutral decay were measured on the Columbia HPD (Hough-Powell device),[4] and subsequently passed through the reconstruction and kinematic fitting programs. It is from these events that we have obtained our data sample corresponding to the reaction

$$K^- p \to \Lambda \eta' \,. \tag{1}$$

Since only two-pronged events with associated neutral decays have been analyzed, we will be discussing only the following two subsets of reaction (1):

$$\begin{aligned} &K^- p \to \Lambda \eta', \\ &\eta' \to \pi^+ \pi^- \eta_N, \\ &\eta_N \to \text{neutrals} \end{aligned} \tag{2}$$